

NOAA Technical Memorandum NOS CS 2

THE RESIDUAL CIRCULATION IN LONG ISLAND SOUND: GYRAL STRUCTURE IN THE CENTRAL AND WESTERN BASINS

Silver Spring, Maryland
October 2003



noaa National Oceanic and Atmospheric Administration

U.S. DEPARTMENT OF COMMERCE
National Ocean Service
Coast Survey Development Laboratory

Office of Coast Survey
National Ocean Service
National Oceanic and Atmospheric Administration
U.S. Department of Commerce

The Office of Coast Survey (CS) is the Nation's only official chartmaker. As the oldest United States scientific organization, dating from 1807, this office has a long history. Today it promotes safe navigation by managing the National Oceanic and Atmospheric Administration's (NOAA) nautical chart and oceanographic data collection and information programs.

There are four components of CS:

The Coast Survey Development Laboratory develops new and efficient techniques to accomplish Coast Survey missions and to produce new and improved products and services for the maritime community and other coastal users.

The Marine Chart Division collects marine navigational data to construct and maintain nautical charts, Coast Pilots, and related marine products for the United States.

The Hydrographic Surveys Division directs programs for ship and shore-based hydrographic survey units and conducts general hydrographic survey operations.

The Navigation Services Division is the focal point for Coast Survey customer service activities, concentrating predominantly on charting issues, fast-response hydrographic surveys and Coast Pilot updates.

THE RESIDUAL CIRCULATION IN LONG ISLAND SOUND: GYRAL STRUCTURE IN THE CENTRAL AND WESTERN BASINS

Richard A. Schmalz, Jr.
Michael F. Devine

October 2003



noaa National Oceanic and Atmospheric Administration

U.S. DEPARTMENT
OF COMMERCE
Donald Evans, Secretary

National Oceanic and
Atmospheric Administration
Conrad C. Lautenbacher, Jr.,
VADM USN (Ret.), Under Secretary

National Ocean Service
Richard Spinrad, Ph.D.
Assistant Administrator

Office of Coast Survey
Captain Roger L. Parsons

Coast Survey Development
Laboratory
Bruce Parker, Ph.D.

NOTICE

Mention of a commercial company or product does not constitute an endorsement by NOAA. Use for publicity or advertising purposes of information from this publication concerning proprietary products or the tests of such products is not authorized.

TABLE OF CONTENTS

FOREWARD	i
INTRODUCTION	1
Physical oceanographic characteristics of the Sound	2
Approach	4
Recent observations and data analysis	4
THE HYDRODYNAMIC MODEL.	5
COMPONENTS OF THE RESIDUAL CIRCULATION.	7
Numerical decomposition	8
Vorticity analysis	15
The residual tidal circulation	17
Density structure and the associated gravitational circulation	18
Wind and sea level effects	19
THE COMPOSITE STRUCTURE OF THE RESIDUAL CIRCULATION	20
The composite model system	21
Seasonal variations	22
Residual currents derived from observations	23
DISCUSSION	25
ACKNOWLEDGEMENTS	27
REFERENCES	27
CONCLUDING REMARKS	45

FOREWARD

On the tenth anniversary of the successful completion of the NOS Long Island Sound Oceanography Project (1988-1994) to further stimulate and encourage research in residual circulation in Long Island Sound a summary paper on this topic is presented here. The paper summarizes the NOS Long Island Sound Project with a focus on residual circulation determination for water quality management. The paper identifies the following areas for further research:

- 1) development of a revised gyral current sampling scheme,
- 2) construction of a higher (0.1-1.0 km horizontal with order 20 sigma level vertical) resolution curvilinear coordinate hydrodynamic model,
- 3) development of a two-dimensional vertically integrated and companion three-dimensional vorticity analysis package, and
- 4) incorporation of the residual circulation computation within the NOS nowcast/forecast system methodology.

To further investigate the gyral circulation, satellite SST and chlorophyll-a structures should be studied. In addition, CODAR and SAR imaging techniques should also be considered.

The Residual Circulation in Long Island Sound: Gyral Structure in the Central and Western Basins

Richard A. Schmalz, Jr. and Michael F. Devine
NOAA/National Ocean Service, N/CS13, 1315 East-West Highway, Silver Spring,
MD, 20910

The nature of the gyral circulation in the central and western Sound is investigated through observations and a three-dimensional numerical model. The National Oceanic and Atmospheric Administration's (NOAA) National Ocean Service (NOS), the State University of New York at Stony Brook (SUNY) and the University of Connecticut (UCONN) observations are used to depict the residual circulation on monthly-averaged time scales. The numerical model provides details of the circulation and its response to external parameters to an extent not previously available. Effects of tides, density fields, winds, and sea level gradients are investigated separately via the numerical model and their contributions to the total residual circulation are presented. Seasonal variations are discussed in terms of an eighteen month simulation and compared with residual currents derived from observations. The gyral structure emerges as a result of the interaction of a stratified tidal estuary with topography. Wind stress modifies the gyral structure considerably, and in six of the eighteen months eliminates it entirely. Recommendations for additional measurement and modeling studies are advanced to further investigate these gyral structures.

INTRODUCTION

Long Island Sound (LIS) has many of the features of a partially mixed estuary. It is about 185 km long and, except near its constricted eastern and western ends, about 15 to 30 km wide. It is divided into eastern (90m maximum depth), central (40m maximum depth) and western (40m maximum depth) basins by a series of irregular sills, as shown in Figure 1. It is distinct from most other estuaries, however, in being connected to the open sea at both ends (through Block Island Sound to the east and the East River and lower Hudson River estuary to the west), and in

having most of its fresh water enter near its eastern, higher salinity end, through the Connecticut and Thames Rivers.

Associated with this structure are some unanswered questions about the residual circulation. In addition to a general eastward flow in the upper layer and westward flow in the lower layer, it has been hypothesized from temperature, salinity and scattered current meter records (Riley, 1952; Paskausky, 1977) that there are mesoscale, horizontal gyral circulations in the western and central Sound. Their nature and permanence, however, have not been extensively observed or analyzed.

Because of these and other uncertainties, and their implications for pollutant loading and transport in Long Island Sound, the National Oceanic and Atmospheric Administration's (NOAA's) National Ocean Service (NOS), the State University of New York at Stony Brook (SUNY), and the University of Connecticut (UCONN) made extensive physical measurements in the Sound in 1988 and 1989. NOS made additional observations (NOS, 1990) and developed a three-dimensional numerical model, which was completed in 1993. The model produced three-dimensional fields of velocity, temperature and salinity at 2.5-minute intervals for the 18-month period from April 1988 through September 1989. Results were used in the Environmental Protection Agency's water quality study of low dissolved oxygen in the western Sound.

Physical oceanographic characteristics of the Sound

The most prominent feature of the water movement in LIS is the tidal current, resulting from a co-oscillating tide wave moving through the Sound. The strongly semi-diurnal tide is primarily progressive as it moves westward through Block Island Sound, but is modified by the bottom topography of LIS in such a way as to gradually change to a primarily standing wave. In the Western Narrows, the dynamics are further complicated by interference from a second tide wave moving up the East River from New York Harbor. The mean tidal range increases from about 0.7 m at The Race to 2.2 m in the Western Narrows. Mean tidal currents are over 200 cm/s in The Race and decrease to less than 25 cm/s in parts of the Western Narrows.

Average surface salinity at Throgs Neck (the western boundary of the Sound) ranges from around 22 psu in the spring to 27 psu in the fall, increasing eastward to 30 to 31 psu at The Race. Bottom salinities are 0.5 to 2 psu higher. A 2 to 4m thick lens of much lower salinity water has been observed to penetrate into the Sound from the Connecticut River during high discharge conditions (Riley, 1956; Garvine, 1986). Thermal stratification develops in the spring and breaks down in the fall. The surface temperatures in the open Sound range from 2 to 5°C in the winter

and from 20 to 25°C in late summer. Bottom temperatures in the summer are 1 to 5 °C lower (Riley, 1956).

The tide, density structure, wind, and sea level in LIS interact with its basin and sill morphology to produce a mean, or residual circulation, with considerable spatial and seasonal variability. Mean residual velocities are generally less than 10 cm/s, except near The Race. The Stokes velocity is important in some parts of LIS, in particular near Throgs Neck and The Race, where Eulerian and Lagrangian velocities and transports may be significantly different (Ianniello, 1981).

Observations by Paskausky and Murphy (1976), Gordon and Pilbeam (1975) and others indicated a general eastward drift near the surface and a westward drift near the bottom, in accord with the conventional structure of gravitational circulation in a partially mixed estuary. However, there were indications of gyral circulations in the basins in the studies of Riley (1952) and Paskausky (1977), which they attributed both to a combination of tidal current interactions with variable depth, the irregular density structure in the central Sound, and the predominantly eastward wind. Irregular and seasonally reversing gravitational circulation in the central Sound was found in a diagnostic two-dimensional model of Wilson (1976). Ianniello (1981) found that 5 to 10 cm/s tidal current residuals may be generated by the strong tidal currents in The Race. Different summer and winter circulation patterns, in response to changing winds, were present in the drifter study of Paskausky and Murphy (1976). The estuarine circulation was weaker in the summer, while near bottom waters moved from the eastern basin into central LIS only in the winter.

Valle-Levinson and Wilson (1994b) have studied the influence of Mattituck sill on the flow field in eastern Sound. They report intratidal and low-pass filtered fluctuations of density stratification and current velocity are due to vertical movement of the halocline and mixed layer growth. During neap tides thin bottom layers are present with significant density stratification, while in contrast during spring tides barotropic rectification becomes important inducing mixed layer growth. They summarize their findings by noting that the residual flow and density fields reflect a change in dynamical balances from spring periods, dominated by frictional stresses to neap periods, where inertial and rotation effects increase and the flow over Mattituck sill may be subject to hydraulic control. Valle-Levinson and Wilson (1994a) performed a series of numerical experiments using a laterally averaged model to study the effect of bathymetry, oscillating barotropic forcing, and vertical mixing on the volume exchange over a simplified Gaussian sill bathymetry based on the Mattituck sill and Long Island Sound length scales. The numerical experiments confirm their observational findings of significant spring to neap variation in the flow.

Approach

We will focus principally on the nature of the gyral circulation in the central and western Sound. Primary attention will be paid to time scales of a month or more. Water movement at these time scales responds to large scale shifts in wind and density patterns, but not to the 3 to 7 day cycle mid-latitude atmospheric variation. Model simulations will show that at these longer time scales, the structure of the gyral circulation undergoes large changes in response to changing external forces. With the aid of the simulations, we will be able to associate these changes with particular external conditions, especially the wind. Observations will also be used to enhance our understanding of Sound circulation.

Recent Observations and data analysis

The NOS field program extended over the periods March 1988 to September 1989 and May to July 1990 and included the following components:

- (1) Acoustic Doppler current profiler (ADCP) current measurements at 25 locations in Long Island Sound, Block Island Sound and the East River,
- (2) Water level measurements from both permanently installed water level stations and stations that were installed specifically for this study, and
- (3) Temperature and conductivity measurements taken in conjunction with several cruises.

In addition to the NOS ADCP measurements (NOS,1990), SUNY made six series of current measurements in LIS. Each series consists of a north to south section of three or four locations, with current meters at three to four depths at each location. The measurement durations ranged from 10 to 40 days (Schmalz et al., 1994).

Both SUNY and UCONN conducted temperature and salinity measurement programs. They made vertical profiles every two to four weeks from April to September 1988 at over 40 locations in LIS and conducted several longitudinal cruises of the Sound. From September 1988 to September 1989, only stations along the Thalweg were occupied at less frequent intervals and were used to calibrate and validate the numerical model (Schmalz et al.,1994).

Because of the high number of returns for each ADCP velocity reading, the ADCP's are able to attain relatively high accuracy; the standard error of the reading is generally reduced to less than 1 cm/s. The effective uncertainty of each reading is then the uncertainty of the instrument itself,

conservatively estimated by the manufacturer to be 1 cm/s. Because of possible contamination from surface effects, bins less than 15% of the station depth from the surface were not used.

The data from each of the processed ADCP bins and SUNY current meters were subjected to a 39-hour Doodson filter (Godin, 1972) to remove the principal tidal frequencies. Because of the large amount of data acquired by each ADCP, only selected depths were completely processed and analyzed, generally five to ten at each location. Depth intervals ranged from 2 meters at shallow stations to 10 meters at the deepest stations. If pressure data were not available, sounded depths were used to obtain an approximate depth below mean low water.

THE HYDRODYNAMIC MODEL

A three-dimensional baroclinic numerical model of LIS was developed to provide details of the circulation and to estimate its response to external parameters to an extent not previously available. The underlying hydrodynamic model employs a general orthogonal curvilinear coordinate system in the horizontal (Blumberg and Herring, 1987) and a bottom and free-surface following sigma (σ) coordinate in the vertical (Blumberg and Mellor, 1980; Blumberg and Mellor, 1987). The vertical mixing (eddy) coefficients, K_M , K_H and K_q are evaluated using the level 2-1/2 turbulence closure model of Mellor and Yamada (1982) as modified by Galperin et al. (1988). Details of the development of these equations are given in Schmalz (1994) and are presented subsequently to introduce the numerical experiments.

The governing equations are approximated via finite differences within an external/internal (barotropic/baroclinic) mode splitting context. All horizontal terms are explicitly differenced with the vertical diffusion terms treated implicitly to afford large internal mode time steps. Details of these procedures are also found in Schmalz (1994). General boundary conditions are discussed in Blumberg and Herring (1987) and in Schmalz (1990).

In application to Long Island Sound, a rectilinear computational grid with 100 cells in the east-west and 37 cells in the north-south directions with a uniform length of 2.032 km was employed (Fig. 2). Seven layers with cell centers at $\sigma = -0.050, -0.141, -0.283, -0.5, -0.717, -0.859,$ and -0.95 were employed in the vertical to resolve depths from 2 to 40 m in the western and central basins (Fig. 3). A 150 second internal mode and 30 second external mode time step or 5:1 mode split was used. Hourly wind data at LaGuardia Airport are assumed to apply for the entire model domain and are adjusted to overwater values using the Hsu (1986) formulation. The spatially uniform windfield approximation over the April 1988 - Sept 1989 period appears reasonable, since monthly average windspeeds at LaGuardia Airport ranged from 4.0 to 6.0 m/s

and at Block Island ranged from 3.8 to 6.4 m/s and differ in any given month by less than 0.9 m/s. The drag coefficient of Large and Pond (1981) is used to compute surface wind stress. Evaporation, precipitation, and atmospheric pressure anomalies were set to zero and sea surface temperature was specified bi-weekly to monthly via patch based inverse distance squared interpolation of surface temperature measurements. Water levels were reconstructed at The Battery, NY and Spuyten Duyvil, NY and along the open boundary in Block Island Sound from 24 tidal constituents and were specified relative to the 1988 North American Vertical Datum (NAVD 1988). Average daily streamflows were input for the five major State of Connecticut rivers (Norwalk River, Mill and Quinnipiac Rivers, Housatonic River, Connecticut River, and Thames Rivers in Fig. 2) and five New York State streams. Sewage treatment plant ($\sim 50 \text{ m}^3/\text{s}$) and combined sewer overflows ($\sim 7 \text{ m}^3/\text{s}$) in New York were also included. For salinity and temperature, a one-dimensional advection equation was used on outflow, while climatological forms (Schmalz, 1992) for salinity and temperature were used on inflow.

A spatially uniform bottom roughness of $z_0 = 1 \text{ cm}$ throughout the Sound and $z_0 = 4 \text{ cm}$ within the Connecticut rivers were calibrated during September 1989 for an astronomical tide simulation initiated from rest with a density field constructed from CTD observations. Rms differences at 13 tide stations between simulated and reconstructed water levels are order 10 cm. Simulated horizontal current components at level 5 (outside near-bottom and near-surface backscatter regions and representative of mid-depth) agree in rms with tidal current components reconstructed from harmonic constituents to within 20% of the tidal current component range. The thermohaline circulation was considered in terms of a 9-month calibration (April - December 1988) and a separate 9-month validation (January - September 1989) using the above calibrated values of bottom roughness. The entire eighteen month period was performed in nine two-month segments. For the initial segment, the initial density fields were developed via interpolation from CTD profiles and the model was spun-up from rest over a one-day period. This one-day period was of sufficient length to establish the tidal response throughout the Sound and to dynamically smooth the initial density fields. All subsequent segments were restarted from the final fields obtained in the previous segment. The magnitude of the rms differences (psu) between 227 observed and computed salinity profiles are nearly the same for the calibration and validation periods at stations A2 (0.70, 0.97) , at H6 (0.56, 0.55), and at M3 (0.73, 0.69) in western, central, and eastern Long Island Sound, respectively (Fig. 2). For stratification index (psu), defined as the absolute value of the difference in stratification between model and data, the comparisons between periods at station A2 (0.60, 0.74), at station H6 (0.37, 0.49), and at station M3 (0.42, 0.51) are all of the same order (Fig. 2). The magnitude of the rms differences ($^{\circ}\text{C}$) between observed and computed temperature profiles are similar for the calibration and validation periods at stations A2 (0.59, 0.77) , at H6 (0.77, 0.82), and at M3 (0.60, 0.53) in western, central, and eastern Long Island

Sound, respectively (Fig. 2). For the stratification index ($^{\circ}\text{C}$), the comparisons between periods are at station A2 (0.69, 0.85), at station H6 (0.67, 0.57), and at station M3 (0.58, 0.31) are again similar (Fig. 2). In general, the longitudinal salinity and temperature gradients both at the near-surface and near-bottom of the Sound are well represented, thus insuring a reasonable representation of the density. Simulated near-surface and near-bottom salinity and temperature fields were compared with observation derived fields for the specific periods April 4 to 7, 1988, June 13 to 16, 1988, and August 2 to 4, 1988 and showed that the general structure of the Connecticut River surface plume and temperature fields were well represented. Additional details of the validation and field comparisons can be found in Schmalz et al. (1994).

COMPONENTS OF THE RESIDUAL CIRCULATION

Tide, density, wind, and mean sea level gradients are all important determinants of the mean residual circulation. Here we examine how each of these factors vary, and how the complete three-dimensional model might be used to evaluate each effect on the residual circulation in Long Island Sound. The present approach seeks to build on previous modeling studies of Long Island Sound performed by Murphy (1980) and to complement recent analytical work conducted by Li and O'Donnell (1997), the results of which we briefly outline.

Murphy (1980) applied a two-dimensional depth-averaged model to Long Island Sound also using a 2 km square grid. Under M_2 tidal forcing, the computed Eulerian residual fields exhibited a clockwise gyre southeast of New Haven, CT, and a convergence to an offshore flow at Stratford Point, CT, in the Central Basin and a counterclockwise gyre east of Eaton's Neck in the Western Basin. To explain the computed fields, he performed the following five additional simulations: 1) best-fit model with advective terms neglected, 2) linearized governing equations with quadratic bottom friction, 3) best-fit model with constant depth of 24m, 4) best-fit model with Coriolis accelerations neglected, and 5) best-fit model with constant depth of 24m and Coriolis acceleration neglected. Based on these simulations, Murphy (1980) concluded that the advective terms played the dominant role in the generation of the tidal residual circulation with depth variation and coastline configuration of next order of importance, followed by the Coriolis acceleration. Murphy (1980) also considered the barotropic response to mean winter (8.5 m/s, 300 deg T) and mean summer (4.5 m/s, 220 deg T) spatially uniform windfields in the absence of tidal forcing. He noted the presence of two gyres with a common westward directed flow ~ 2 cm/s in winter and ~ 0.5 cm/s in summer in the Central Basin deep channel. The inner limbs of the gyres in the near-shore regions were cyclonic off Connecticut and anti-cyclonic off Long Island at current strengths of ~ 5 cm/s in winter and ~ 1.3 cm/s in summer.

Li and O'Donnell (1997) recently reviewed the application of perturbation methods for solving the two-dimensional, depth-averaged equations in simplified estuarine geometries and extended the method to a straight constant width channel with lateral depth variations under single constituent tidal forcing. They found inward residual flow over the shoals and a net outflow in the channel. They note the difficulties of extending these results to real estuaries, particularly of large width such as Long Island Sound.

For the purposes of this paper, the observed residual velocity will be defined as that remaining after the low pass filters described above have been applied to the velocity record. The mean residual velocity is then the time average of the computed residuals. In the model, the Eulerian residual circulation is computed by dividing the internal mode transport per unit width at each sigma level averaged over one hour by the averaged internal mode depth over a one hour period and then averaging these hourly sigma level quotients over the complete month.

Numerical Decomposition

To set the stage for the numerical experiments, consider the following sigma coordinate transformation. The internal mode equations in sigma coordinates become:

$$(x' = x, y' = y, \sigma = \frac{z - \eta}{H}); \frac{dx'}{dt} = u; \quad \frac{dy'}{dt} = v; \quad \omega = H \frac{d\sigma}{dt} \quad (1)$$

$$\frac{\partial \eta}{\partial t} + \frac{\partial(Hu)}{\partial x'} + \frac{\partial(Hv)}{\partial y'} + \frac{\partial \omega}{\partial \sigma} = 0 \quad (2a)$$

$$\begin{aligned} \frac{\partial(Hu)}{\partial t} + \frac{\partial(Hu^2)}{\partial x'} + \frac{\partial(Huv)}{\partial y'} + \frac{\partial(\omega u)}{\partial \sigma} &= fHv - gH \frac{\partial \eta}{\partial x'} - \frac{H}{\rho_o} \frac{\partial P_a}{\partial x'} \\ &+ \frac{gH}{\rho_o} \frac{\partial H}{\partial x'} \int_{\sigma}^0 \frac{\partial \rho}{\partial \sigma} d\sigma - \frac{gH^2}{\rho_o} \frac{\partial}{\partial x'} \left[\int_{\sigma}^0 \rho d\sigma \right] + \frac{\partial \tau_{x'x'}}{\partial x'} + \frac{\partial}{\partial \sigma} \left[\frac{\partial \sigma}{\partial x} \tau_{x'x'} \right] \\ &+ \frac{\partial \tau_{y'x'}}{\partial y'} + \frac{\partial}{\partial \sigma} \left[\frac{\partial \sigma}{\partial y} \tau_{y'x'} \right] + H^{-1} \frac{\partial}{\partial \sigma} \left(K_m \frac{\partial u}{\partial \sigma} \right) \end{aligned} \quad (2b)$$

$$\begin{aligned}
\frac{\partial(Hv)}{\partial t} + \frac{\partial(Hvu)}{\partial x'} + \frac{\partial(Hv^2)}{\partial y'} + \frac{\partial(\omega v)}{\partial \sigma} &= -fHu - gH \frac{\partial \eta}{\partial y'} - \frac{H}{\rho_o} \frac{\partial P_a}{\partial y'} \\
&+ \frac{gH}{\rho_o} \frac{\partial H}{\partial y'} \int_{\sigma}^0 \frac{\partial \rho}{\partial \sigma} d\sigma - \frac{gH^2}{\rho_o} \frac{\partial}{\partial y'} \left[\int_{\sigma}^0 \rho d\sigma \right] + \frac{\partial \tau_{x'y'}}{\partial x'} + \frac{\partial}{\partial \sigma} \left[\frac{\partial \sigma}{\partial x} \tau_{x'y'} \right] \\
&+ \frac{\partial \tau_{y'y'}}{\partial y'} + \frac{\partial}{\partial \sigma} \left[\frac{\partial \sigma}{\partial y} \tau_{y'y'} \right] + H^{-1} \frac{\partial}{\partial \sigma} \left(K_m \frac{\partial v}{\partial \sigma} \right)
\end{aligned} \tag{2c}$$

$$\begin{aligned}
\frac{\partial(HT)}{\partial t} + \frac{\partial(HuT)}{\partial x'} + \frac{\partial(HvT)}{\partial y'} + \frac{\partial(\omega T)}{\partial \sigma} &= \frac{\partial Q_{x'T}}{\partial x'} \\
&+ \frac{\partial}{\partial \sigma} \left[\frac{\partial \sigma}{\partial x} Q_{x'T} \right] + \frac{\partial Q_{y'T}}{\partial y'} + \frac{\partial}{\partial \sigma} \left[\frac{\partial \sigma}{\partial y} Q_{y'T} \right] + H^{-1} \frac{\partial}{\partial \sigma} \left(K_H \frac{\partial T}{\partial \sigma} \right)
\end{aligned} \tag{2d}$$

$$\begin{aligned}
\frac{\partial(HS)}{\partial t} + \frac{\partial(HuS)}{\partial x'} + \frac{\partial(HvS)}{\partial y'} + \frac{\partial(\omega S)}{\partial \sigma} &= \frac{\partial Q_{x'S}}{\partial x'} \\
&+ \frac{\partial}{\partial \sigma} \left[\frac{\partial \sigma}{\partial x} Q_{x'S} \right] + \frac{\partial Q_{y'S}}{\partial y'} + \frac{\partial}{\partial \sigma} \left[\frac{\partial \sigma}{\partial y} Q_{y'S} \right] + H^{-1} \frac{\partial}{\partial \sigma} \left(K_H \frac{\partial S}{\partial \sigma} \right)
\end{aligned} \tag{2e}$$

$$\begin{aligned}
\frac{\partial(q^2 H)}{\partial t} + \frac{\partial(q^2 Hu)}{\partial x'} + \frac{\partial(q^2 Hv)}{\partial y'} + \frac{\partial(q^2 \omega)}{\partial \sigma} &= \frac{\partial Q_{x'q^2}}{\partial x'} \\
&+ \frac{\partial}{\partial \sigma} \left[\frac{\partial \sigma}{\partial x} Q_{x'q^2} \right] + \frac{\partial Q_{y'q^2}}{\partial y'} + \frac{\partial}{\partial \sigma} \left[\frac{\partial \sigma}{\partial y} Q_{y'q^2} \right] + H^{-1} \frac{\partial}{\partial \sigma} \left(K_q \frac{\partial q^2}{\partial \sigma} \right) \\
&+ 2 \frac{K_m}{H} \left[\left(\frac{\partial u}{\partial \sigma} \right)^2 + \left(\frac{\partial v}{\partial \sigma} \right)^2 \right] + \frac{2g}{\rho_o} K_H \frac{\partial \rho}{\partial \sigma} - \frac{2Hq^3}{B_1 l}
\end{aligned} \tag{2f}$$

$$\begin{aligned}
& \frac{\partial(q^2 \ell H)}{\partial t} + \frac{\partial(q^2 \ell Hu)}{\partial x'} + \frac{\partial(q^2 \ell Hv)}{\partial y'} + \frac{\partial(q^2 \ell \omega)}{\partial \sigma} = \frac{\partial Q_{x' q^2 \ell}}{\partial x'} \quad (2g) \\
& + \frac{\partial}{\partial \sigma} \left[\frac{\partial \sigma}{\partial x} Q_{x' q^2 \ell} \right] + \frac{\partial Q_{y' q^2 \ell}}{\partial y'} + \frac{\partial}{\partial \sigma} \left[\frac{\partial \sigma}{\partial y} Q_{y' q^2 \ell} \right] + H^{-1} \frac{\partial}{\partial \sigma} \left(K_q \frac{\partial q^2 \ell}{\partial \sigma} \right) \\
& + \frac{\ell E_1 g}{\rho_o} K_H \frac{\partial \rho}{\partial \sigma} - \frac{H q^3}{B_1} \omega + \ell E_1 \frac{K_m}{H} \left[\left(\frac{\partial u}{\partial \sigma} \right)^2 + \left(\frac{\partial v}{\partial \sigma} \right)^2 \right]
\end{aligned}$$

Supplemental relations used in the above equations are as follows.

$$\tau_{x'y'} = \tau_{y'x'} = A_M \left[\frac{\partial(uH)}{\partial y'} + \frac{\partial}{\partial \sigma} \left(Hu \frac{\partial \sigma}{\partial y} \right) + \frac{\partial(vH)}{\partial x'} + \frac{\partial}{\partial \sigma} \left(Hv \frac{\partial \sigma}{\partial x} \right) \right] \quad (3a)$$

$$\tau_{x'x'} = 2 A_M \left[\frac{\partial(uH)}{\partial x'} + \frac{\partial}{\partial \sigma} \left(Hu \frac{\partial \sigma}{\partial x} \right) \right]; \quad \tau_{y'y'} = 2 A_M \left[\frac{\partial(vH)}{\partial y'} + \frac{\partial}{\partial \sigma} \left(Hv \frac{\partial \sigma}{\partial y} \right) \right]$$

$$-H \frac{\partial \sigma}{\partial x} = \sigma \frac{\partial H}{\partial x'} + \frac{\partial \eta}{\partial x'}; \quad -H \frac{\partial \sigma}{\partial y} = \sigma \frac{\partial H}{\partial y'} + \frac{\partial \eta}{\partial y'} \quad (3b)$$

$$Q_{x'T} = A_H \left[\frac{\partial(TH)}{\partial x'} + \frac{\partial}{\partial \sigma} \left(HT \frac{\partial \sigma}{\partial x} \right) \right]$$

$$Q_{y'T} = A_H \left[\frac{\partial(TH)}{\partial y'} + \frac{\partial}{\partial \sigma} \left(HT \frac{\partial \sigma}{\partial y} \right) \right]$$

where similar relations hold for $Q_{x'S}$, $Q_{y'S}$, $Q_{x'q^2}$, $Q_{y'q^2}$, $Q_{x'q^2\ell}$, and $Q_{y'q^2\ell}$.

In Equations 1-3, the variables are as defined as follows:

- (x,y,z) \equiv east, north, and vertical coordinates, respectively,
 (x',y',σ) \equiv transformed east, north, and vertical coordinates, respectively,
 (u,v,ω) \equiv x' , y' , and σ velocity components, respectively,
 t \equiv time,
 f \equiv Coriolis parameter,
 H \equiv total water depth,
 η \equiv water surface elevation with respect to model datum,
 ρ \equiv water density,
 ρ_o \equiv reference water density,
 P_a \equiv sea-level atmospheric pressure,
 g \equiv gravitational acceleration,
 T \equiv temperature,
 S \equiv salinity,
 $q'/2$ \equiv turbulent kinetic energy,
 l \equiv turbulent length scale,
 $\tau_{x'x'}, \tau_{x'y'}, \tau_{y'x'}, \tau_{y'y'}$ \equiv Reynolds stresses,
 $Q_{x'T}, Q_{y'T}$ \equiv temperature horizontal diffusion terms,
 $Q_{x'S}, Q_{y'S}$ \equiv salinity horizontal diffusion terms,
 ω \equiv wall function,
 (E_1, B_1) \equiv empirical turbulent parameters,
 A_M \equiv horizontal momentum mixing coefficient,
 K_m \equiv vertical momentum mixing coefficient,
 A_H \equiv horizontal constituent mixing coefficient
 K_H \equiv vertical salinity or temperature mixing coefficient, and
 K_q \equiv vertical turbulence constituent mixing coefficient.

Next consider the external-mode equations, where $(\bar{u}, \bar{v}) = \begin{pmatrix} 0 & 0 \\ \int_{-1}^0 u d\sigma & \int_{-1}^0 v d\sigma \end{pmatrix}$ and

$$\bar{A}_M = \int_{-1}^0 A_M d\sigma \text{ with } (\tau_{xS}, \tau_{yS}), (\tau_{xb}, \tau_{yb}) \text{ as surface and bottom stresses, respectively.}$$

$$\frac{\partial \eta}{\partial t} + \frac{\partial(\bar{u}H)}{\partial x'} + \frac{\partial(\bar{v}H)}{\partial y'} = 0 \quad (4a)$$

$$\frac{\partial(H\bar{u})}{\partial t} + \frac{\partial(H\bar{u}\bar{u})}{\partial x'} + \frac{\partial(H\bar{u}\bar{v})}{\partial y'} = fH\bar{v} \quad (4b)$$

$$\begin{aligned} & - gH \frac{\partial \eta}{\partial x'} - \frac{H}{\rho_o} \frac{\partial P_a}{\partial x'} + \frac{gH}{\rho_o} \frac{\partial H}{\partial x'} I_1 - \frac{gH^2}{\rho_o} \frac{\partial I_2}{\partial x'} \\ & + \frac{\tau_{xs}}{\rho_o} - \frac{\tau_{xb}}{\rho_o} + \frac{\partial}{\partial x'} \left(2\bar{A}_M \frac{\partial(\bar{u}H)}{\partial x'} \right) + \frac{\partial}{\partial y'} \left(\bar{A}_M \left(\frac{\partial(\bar{u}H)}{\partial y'} + \frac{\partial(\bar{v}H)}{\partial y'} \right) \right) \end{aligned}$$

$$\frac{\partial(H\bar{v})}{\partial t} + \frac{\partial(H\bar{v}\bar{u})}{\partial x'} + \frac{\partial(H\bar{v}\bar{v})}{\partial y'} = -fH\bar{u} \quad (4c)$$

$$\begin{aligned} & - gH \frac{\partial \eta}{\partial y'} - \frac{H}{\rho_o} \frac{\partial P_a}{\partial y'} + \frac{gH}{\rho_o} \frac{\partial H}{\partial y'} I_1 - \frac{gH^2}{\rho_o} \frac{\partial I_2}{\partial y'} \\ & + \frac{\tau_{ys}}{\rho_o} - \frac{\tau_{yb}}{\rho_o} + \frac{\partial}{\partial y'} \left(2\bar{A}_M \frac{\partial(\bar{v}H)}{\partial y'} \right) + \frac{\partial}{\partial x'} \left(\bar{A}_M \left(\frac{\partial(\bar{u}H)}{\partial y'} + \frac{\partial(\bar{v}H)}{\partial x'} \right) \right) \end{aligned}$$

Note

$$I_1 = \int_{-1}^0 \int_{\sigma'}^0 \sigma \frac{\partial \rho}{\partial \sigma} d\sigma d\sigma' \quad I_2 = \int_{-1}^0 \int_{\sigma'}^0 \rho d\sigma d\sigma'.$$

For purposes of characterizing the finite difference equations, we next introduce the following representations for the external and internal modes, wherein it is understood that the left-most term of the left-hand side represents the given hydrodynamic variable at time $n\Delta T_E$ for the external mode and at time $m\Delta T_I$ for the internal mode, $mM\Delta T_E = m\Delta T_I$, for mode split M .

Note for hydrodynamic variable, h , h_{ELi} and h_{ERi} denote external mode finite difference approximations to the i th terms on the left and right hand sides, respectively, in the above equations. A similar approach is followed for the internal mode finite difference approximations (refer to Blumberg and Mellor (1987)). The finite difference approximations may then be written as:

$$\begin{aligned}
(4a) \quad \eta_I + \sum_{l=1}^4 \eta_{IL_l} &= 0 & (2a) \quad \eta_E + \sum_{l=1}^3 \eta_{EL_l} &= 0 \\
(4b) \quad U_I + \sum_{l=1}^4 U_{IL_l} &= \sum_{l=1}^{10} U_{IR_l} & (2b) \quad U_E + \sum_{l=1}^3 U_{EL_l} &= \sum_{l=1}^9 U_{ER_l} \\
(4c) \quad V_I + \sum_{l=1}^4 V_{IL_l} &= \sum_{l=1}^{10} V_{IR_l} & (2c) \quad V_E + \sum_{l=1}^3 V_{EL_l} &= \sum_{l=1}^9 V_{ER_l} \\
(2d) \quad S_I + \sum_{l=1}^4 S_{IL_l} &= \sum_{l=1}^5 S_{IR_l} & (2e) \quad T_I + \sum_{l=1}^4 T_{IL_l} &= \sum_{l=1}^5 T_{IR_l} \\
(2f) \quad q^2 I_I + \sum_{l=1}^4 q^2 I_{IL_l} &= \sum_{l=1}^8 q^2 I_{IR_l} & (2g) \quad q^2 E + \sum_{l=1}^4 q^2 E_{IL_l} &= \sum_{l=1}^8 q^2 E_{IR_l}
\end{aligned} \tag{5}$$

With respect to the above equation set, we consider the six following α denoted reduced equation sets. For $\alpha_1 = 0$, the horizontal advection terms in the external mode equations $U_{EL_2} = U_{EL_3} = V_{EL_2} = V_{EL_3} = 0$. For the internal mode the horizontal advection terms $U_{IL_2} = U_{IL_3} = V_{IL_2} = V_{IL_3} = 0$, while vertical advection is retained.

For $\alpha_2 = 0$, the horizontal density gradients in the external mode momentum equations $U_{EL_4} = U_{EL_5} = V_{EL_4} = V_{EL_5} = 0$. For the internal mode the horizontal density gradient terms $U_{IL_4} = U_{IL_5} = V_{IL_4} = V_{IL_5} = 0$.

For $\alpha_3 = 0$, the horizontal advection terms in the temperature and salinity internal mode equations $T_{IL_2} = T_{IL_3} = S_{IL_2} = S_{IL_3} = 0$, thereby removing their influence on density.

For $\alpha_4 = 0$, the Coriolis effects $U_{EL_1} = V_{EL_1} = U_{IL_1} = V_{IL_1} = 0$.

For $\alpha_5 = 0$, the vertical mixing terms in the salinity and temperature $S_{IL_5} = T_{IL_5} = 0$.

For $\alpha_6 = 0$, the vertical mixing terms in the turbulence quantities $q^2_{IL_5} = q^2 I_{IL_5} = 0$.

$$\text{Next consider } \langle U_I \rangle_{\alpha_1=0} = \left\langle \sum_{i=1}^{10} U_{IR_i} - \sum_{i=2,3}^4 U_{IL_i} \right\rangle \quad \langle V_I \rangle_{\alpha_1=0} = \left\langle \sum_{i=1}^{10} V_{IR_i} - \sum_{i=2,3}^4 V_{IL_i} \right\rangle$$

in which $U_{EL_1} = U_{EL_2} = U_{IL_1} = U_{IL_2} = V_{EL_1} = V_{EL_2} = V_{IL_1} = V_{IL_2} = 0$ to form the reduced equation set and $\langle \rangle$ represents a temporal average operator (one month).

$$\text{First considering } U_I, \quad \langle U_I \rangle_{\alpha_1} = \sum_{i=1}^{10} \langle U_{IR_i} \rangle - \sum_{i=2,3}^4 \langle U_{IL_i} \rangle \text{ in which the complete}$$

hydrodynamic equations are used but with the influence of the terms dropped previously not retained. For a nonlinear system, $\langle U_I \rangle_{\alpha_1=0} \neq \langle U_I \rangle_{\alpha_1}$, with the absolute value of the factor

$f_{\alpha_1} = (\langle U_I \rangle_{\alpha_1=0} - \langle U_I \rangle_{\alpha_1}) / \langle U_I \rangle_{\alpha_1}$, representing the degree of nonlinearity of U_I with respect to the α_1 terms. Analogous remarks hold for the V_I component. In this study, we have considered the $\alpha_2=0$ case to assess the horizontal density gradient terms, and have assumed a weak nonlinearity. In this case, we have further assumed that the horizontal density gradient effect is representative of a density or gravitational circulation. Additional density circulation representations are possible; e.g., $\alpha_2 + \alpha_5 = 0$, $\alpha_3 + \alpha_5 = 0$, $\alpha_2 + \alpha_5 + \alpha_6 = 0$, and $\alpha_3 + \alpha_5 + \alpha_6 = 0$.

The above analysis is contingent upon the initial and boundary conditions. The initial density field is seasonally dependent, as is wind and subtidal water level boundary conditions. In the present work, we have considered April 1988 conditions to represent an annual average and have computed the α_2 case in the absence of wind and subtidal water level forcings as a first step.

The water surface elevation boundary conditions consist of the astronomical tide (A) plus the subtidal water level (S), which is assumed to reflect the influence of non-local wind. The local wind effect (W) is obtained by setting surface wind stresses based on a spatially uniform windfield. We thus numerically decompose the monthly averaged Eulerian residual circulation as follows:

$$C(A,S,W,D) = C(W) + C(S) + C(A) + C(D) \quad (6)$$

where

$C(A,S,W,D)$ = Eulerian residual circulation with astronomical tide, subtidal water level (sea slope), wind, and density forcings.

$C(A,W,D)$ = Eulerian residual circulation with astronomical tide, wind, and density forcings.

$C(A,S,D)$ = Eulerian residual circulation with astronomical tide, subtidal water level (sea slope), and density forcings.

$C(A,D)$ = Eulerian residual circulation with astronomical tide and density forcing.

$C(A)$ = Eulerian residual circulation with astronomical tide with α_2 terms zero, which is assumed to estimate the average Eulerian astronomical tide circulation.

$C(D)$ = Eulerian residual density circulation estimate.

$C(W)$ = Eulerian residual local wind circulation estimate.

$C(S)$ = Eulerian residual non-local wind (sea slope) circulation estimate.

Note $C(A,D) = C(A) + C(D)$, where $C(D) = C(A,D) - C(A)$.

$$C(W) = C(A,S,W,D) - C(A,S,D)$$

$$C(S) = C(A,S,W,D) - C(A,W,D) = C(A,S,D) - C(A,D)$$

Note we might also consider that, $C(A,D) + C(S) = C(A,S,D) = C(A,S) + C(S,D)$, where $C(A,S) = C(A,S,D)_{\alpha_2=0}$, and $C(S,D) = C(A,S,D) - C(A,S)$. In this case, we assume $C(A,S) = C(S) + C(A)$, $C(W) = C(A,S,W,D) - C(A,S,D)$, and that $C(S,D) \sim C(D)$ to obtain a balance.

If we consider $C(A,S,W,D) = C(A,S,W) + C(A,S,D)$, where $C(A,S,W) = C(A,S,W,D)_{\alpha_2=0}$, and $C(A,S,D) = C(A,S,W,D) - C(A,S,W)$, then we assume $C(A,S,W) = C(A) + C(S) + C(W)$ and that $C(A,S,D) \sim C(D)$ to obtain a balance.

Under these assumptions, the complete circulation may be numerically decomposed as performed herein. Additional numerical experiments are needed to further confirm the degree of nonlinearity and hence error in these assumptions. The error must be evaluated in terms of relative difference as well as in flow pattern characteristics. The hypothesis here is that while locally differences may be relatively large, over basin scales the flow pattern characteristics will be similar, and hence will be useful in qualitatively describing the component circulations.

The above must be evaluated on an estuary by estuary basis, and if the degree of nonlinearity is large such that the above assumptions do not hold, then one may not consider the circulation on a component basis and a vorticity balance approach is necessary. Such an approach is useful in its own right and is presented below.

Vorticity Analysis

In a cartesian frame, $\mathbf{W} = \nabla \times \mathbf{U} = (\partial w / \partial y - \partial v / \partial z)\mathbf{i} + (\partial w / \partial x - \partial u / \partial z)\mathbf{j} + (\partial v / \partial x - \partial u / \partial y)\mathbf{k}$ and one must consider rotations about the x, y, and z axes. To develop the complete vorticity balance equations, one should perform the above operations with respect to each axis, employing the cartesian hydrodynamic set. Upon forming the derivatives, a change to sigma coordinates would need to be made. The k component equations so obtained would be approximated via finite differences in a separate vorticity analysis package compatible with the Long Island Sound hydrodynamic model to evaluate the horizontal vorticity balance.

Here, we consider the external mode momentum equations vertically integrated in sigma coordinates and evaluate the vorticity about \mathbf{k} by forming $\partial(\cdot) / \partial x'$ of the v momentum and subtracting $\partial(\cdot) / \partial y'$ of the u momentum equation as discussed by Robinson (1980) and

Zimmerman (1978). The wind stress and sigma coordinate density integrals are included to obtain the following relation in which the prime notations are dropped:

$$\begin{aligned}
 \frac{\partial \omega}{\partial t} + u \frac{\partial \omega}{\partial x} + v \frac{\partial \omega}{\partial y} + \omega \left(\frac{\partial u}{\partial x} + \frac{\partial v}{\partial y} \right) &= -f \left(\frac{\partial u}{\partial x} + \frac{\partial v}{\partial y} \right) \\
 \text{-----1-----} & \quad \text{-----2-----} \quad \text{-----3-----} \\
 + \frac{g}{\rho_0} \left(\frac{\partial H}{\partial y} \left(\frac{\partial I_1}{\partial x} - \frac{\partial I_2}{\partial x} \right) - \frac{\partial H}{\partial x} \left(\frac{\partial I_1}{\partial y} - \frac{\partial I_2}{\partial y} \right) \right) & \\
 \text{-----4-----} & \quad \text{-----5-----} \\
 + \frac{1}{\rho_0 H} \left(\frac{\partial \tau_{ys}}{\partial x} - \frac{\partial \tau_{xs}}{\partial y} \right) - \frac{1}{\rho_0 H^2} \left(\frac{\partial H}{\partial x} \tau_{ys} - \frac{\partial H}{\partial y} \tau_{xs} \right) & \\
 \text{-----6-----} & \quad \text{-----7-----} \\
 + (u^2 + v^2)^{0.5} \left(u \frac{\partial C_D / H}{\partial y} - v \frac{\partial C_D / H}{\partial x} \right) + C_D / H \left(u \frac{\partial (u^2 + v^2)^{0.5}}{\partial y} - v \frac{\partial (u^2 + v^2)^{0.5}}{\partial x} \right) & \\
 \text{-----8-----} & \quad \text{-----9-----} \\
 - C_D / H (u^2 + v^2)^{0.5} \omega + v \nabla^2 \omega & \\
 \text{-----10-----} & \quad \text{-----11-----}
 \end{aligned} \tag{7}$$

Note $\omega = \partial v / \partial x - \partial u / \partial y$ is the relative vorticity, C_D is a bottom friction coefficient, v is a relative vorticity dissipation coefficient, and the other terms are as defined previously. The terms denoted 1-11 denote, respectively: 1) the material derivative of vorticity (tendency and advection), 2) relative vortex stretching, 3) planetary vortex stretching, 4) x-direction density integral gradient, 5) y-direction density integral gradient, 6) surface stress gradient, 7) depth gradient surface stress product, 8) differential bottom friction by the slope of the bottom perpendicular to the direction of the current, 9) differential bottom friction by differences in current, 10) damping of vorticity by bottom friction, and 11) lateral diffusion of vorticity.

Vorticity is produced by planetary vortex stretching when the current flows in the direction of the bottom slope or by differential bottom friction when the current is along the isobaths. Once generated, vorticity can be rectified by either advection or relative vortex stretching. The advective rectification process redistributes the relative vorticity while relative vortex stretching is a local process where cross-isobath currents traverse large bottom slopes.

For the three-dimensional situation three flow regimes will need to be considered. In region 1, representing the surface boundary layer, the surface stresses will be introduced. Similarly, in region 3 representing the bottom boundary layer, the bottom stress will be introduced resulting in terms similar to 8-10, above. In the interior flow region 2, vertical velocity gradients will interact with horizontal gradients in the vertical mixing coefficient K_m .

The residual tidal circulation

The general characteristics of the tidal circulation are first considered. Numerical simulations (Sun, 1992; Wei, 1993) have confirmed these characteristics and added considerable detail on phase and amplitude. Model results are generally in good agreement with NOS tidal current tables; the average rms differences are 20 and 21 cm/s for mean maximum flood and ebb currents, respectively. Tidal currents are mostly reversing, but some rotary characteristics are present in the central basin Thalweg, with the ratio of the minor axis to the major axis as large as 0.15. The principal lunar semidiurnal constituent (M_2) is the dominant tidal current constituent in all parts of the Sound. In some parts of the open Sound, however, the sum of the larger lunar elliptic semidiurnal constituent and the principal solar semidiurnal constituent (N_2+S_2) can be half as large as M_2 , and in the Western Narrows the sum of the first even and odd harmonic (M_4+M_6) can be this large as well.

The ADCP observations show considerable vertical structure to the tidal currents. The M_2 ellipses in the lower layers of the eastern Sound are considerably attenuated and flattened relative to those at the surface; both tendencies are less in the central and western Sound. Lower layer phases are almost the same as those near the surface in The Race, but become 20 to 30 minutes earlier in the central and western Sound. Sun (1992) demonstrated a high predictive skill (greater than 0.9) for the hydrodynamic model in representing the vertical variation of east component of the tidal currents at stations 8 and 9 (Fig. 2).

Since the tidal residual components in the velocity record cannot be straightforwardly separated from each other or from density effects, the hydrodynamic model was used to accomplish this for April 1988, in which initial salinity and temperature conditions were constructed via an inverse distance interpolation based on 25 observed salinity and temperature profiles. To look at the effects of the tide interacting with the topography in isolation, the horizontal density gradient terms in the horizontal pressure gradient were set to zero in the external and internal mode horizontal momentum equations (C(A)). Note density effects are still present in the vertical mixing terms. Figure 4 shows the near-surface and near-bottom mean tidal current residuals in the western and central basins. In these and the corresponding following figures, only velocities equal to or less than the scale arrow length are indicated, so as to illustrate the gyral circulations as clearly as possible. Note that different scales are used for near-surface (2m) and near-bottom flow (-2m). At a depth of 10 m, which is only at or near the bottom close to the Connecticut and Long Island shores and represents a mid-depth in most regions (Fig. 3), the gyral structure is weaker and more complex and is not shown but will be summarized.

The model simulation shows distinct near-surface cyclonic gyres in the western and central basins, with near-surface gyral velocities as high as 10 to 15 cm/s. Wilson (unpublished) has obtained similar near-surface cyclonic tide induced gyral patterns in the Central and Western basins. In the NOS simulation, the pattern of these gyres was also present at 10m. The gyres were not found in the NOS simulated near-bottom flow; the simulated flow there is mostly weak and variable, except for moderate westward flow in the western part of the Thalweg, and generally stronger westward and southward flow near Mattituck Sill, mostly opposite to the near-surface flow.

Ridderinkhof and Zimmerman (1990) in an application of the vertically-integrated flow vorticity balance in the Western Dutch Wadden Sea, note that vortex stretching was a production agency for residual vorticity due to an asymmetry in the vorticity dynamics at the sides of the channel (thalweg) and nearshore. Differential bottom friction produced a strong shear layer with vorticity of alternating sign during the tidal cycle, while vortex stretching changed sign as well. During the flood, when differential bottom friction created relative vorticity along the sides of the thalweg, the associated relative vortex columns were compressed as they moved out of the main channel toward the shallow near-shore regions, which was thus a negative feedback. During the ebb, however, the ebb currents created strong vorticity along the channel (thalweg) sides, concurrently stretching the vortex columns as the water left the shallow regions, resulting in a positive feedback, which when averaged over the tidal cycle resulted in a production of residual vorticity. In the central and western basins of Long Island Sound, for the tidal case terms 6 and 7 in the vorticity equation are zero, and it is hypothesized that vorticity is generated via term 8 with terms 9 and 10 acting to hamper generation. The density integral terms also serve to reduce vorticity near the Connecticut and Long Island shores. The stretching terms also modify the balance through the mechanism reported above by Ridderinkhof and Zimmerman (1980), such that in the mid-regions of both basins a region of positive residual vorticity is achieved manifesting the presence of two cyclonic gyres. At present, the above is a hypothesis and must be confirmed via further study and evaluation of the terms in the vorticity balance. As there is considerable variation over the vertical of the residual fields, vertical gradients of the horizontal velocity components and of the vertical mixing coefficient along with the frictional damping confined to the bottom layers will tend to redistribute the horizontal balance.

Density structure and the associated gravitational circulation

Extensive observations of temperature and salinity in LIS were made by SUNY and UCONN between April and September 1988. After September, observations were more sparse. In April (Fig. 5), the general west to east increase in salinity is interrupted both by a weak salinity minimum in the central basin and by minima near Connecticut associated with outflow from the

Housatonic and Connecticut Rivers. Salinity also generally increased from west to east later in the stratified season, but the gradient was again reversed over several tens of kilometers in the central Sound during August.

In early April (Fig. 6), seasonal thermal stratification has not yet begun; the thermocline began to develop later in April, and a complex stratified structure was evident by June. By early August, the thermal stratification was over 5°C throughout most of the Sound, but by mid-August the thermal structure was breaking down. By mid-September, there was no stratification. The isopycnal structure in the north-south section across the Sound in April shows freshwater influence near the Connecticut and Long Island coastlines, producing the characteristic inverted "U" shape with depth in the center of the Sound. The density structure across the central Sound was more complex in June and August, with several maxima and minima across the Sound. The seasonal thermohaline structure is discussed further in Schmalz et al. (1994).

By an indirect procedure, the model can be used to consider the effects of density gradients, without tidal residuals. The model, having previously been run with tide alone, ($C(A)$), is now run with tide plus density ($C(A,D)$); the circulation with density alone ($C(D)$) is then estimated as the difference ($C(D) = C(A,D) - C(A)$). During April 1988, which is a month of low-stratification with no seasonal thermocline, the near-surface density induced velocity (Fig. 7) shows central and western basin cyclonic gyres similar to those induced by the tide, but somewhat weaker; the strongest flow is over Mattituck Sill. In addition, there is eastward flow near Long Island and westward flow near Connecticut, consistent with the density structure (Fig. 6). At 10 m there is a strong cyclonic gyre near Mattituck Sill; the gyres in the main basins are weak. Near the bottom, the gyres are absent but a 5 cm/s eastward flow over Mattituck Sill and near Long Island exists. The model deduced near-surface residual density circulation is consistent with the density circulation of Long Island Sound hypothesized by Pritchard (1990), in which surface flow along the Connecticut shoreline is to the east with an opposite-directed surface flow along the Long Island shoreline. The near-bottom residual circulation described by the model is directed to the east across the entire Sound in general agreement to that suggested by Pritchard (1990), who notes a band of westward directed flow confined to the Connecticut shoreline, which is not present in the model.

Wind and sea level effects

Neither wind stress nor sea slope ever acts in isolation; as in the previous sections however, we can use the model to isolate each effect. Computationally, the wind effects alone ($C(W)$) are derived by subtracting a simulation, which includes tide, density and sea level effects but zero

wind stress $C(A,S,D)$ from a simulation including wind stress, sea level, tide, and density effects ($C(A,S,W,D)$). Similarly, sea surface slope effects alone ($C(S)$) are derived by subtracting a simulation in which the Montauk-Battery sea level difference is set to zero (but with tide, density, and wind stress included) from the simulation including all four effects ($C(A,S,W,D) - C(A,W,D)$).

Model-generated mean near-surface and near-bottom vectors for the presumably non-locally-caused April 1988 sea level difference between Montauk and The Battery of -3.0 cm with no local wind were first examined. These vectors are insignificant and plot only as dots at 15 cm/s and 5 cm/s scales, respectively. While an order 3.0 cm change in mean sea level difference over the Sound does not influence basin scale residual circulation patterns, it does effect the mean flow from Long Island Sound through the East River. Blumberg and Pritchard (1997) report that a 1 cm change in water surface elevation between The Battery and Willets Point changes the mean flow through the East River by 46 m³/s, roughly a sixth of its long term average.

Near-surface and near-bottom vectors for local wind alone (with a zero Montauk-Battery sea level difference) in April 1988 when the monthly mean wind at LGA was 1 m/s southeastward were then considered (Fig. 8). In this case, the local wind alone ($C(W)$) generates a more energetic, near-surface circulation pattern quite different from the tide plus density ($C(A,D)$) picture. Anticyclonic gyres are present in the central and western basins, in contrast to the cyclonic gyres generated by tide and density. At 10 m the wind-driven flow is much weaker, except in the Thalweg. Near-bottom currents are still weaker. Eastward flow near Connecticut persists throughout the water column as does the return flow in the Thalweg. In contrast with the vertically-integrated model results of two counter-directed gyres in the near-shore regions (Murphy, 1980), only a single cyclonic gyre is present. However in the vertically-integrated model all adjustments must be made laterally and no bottom layer return flow is possible.

The wind-driven velocity structure in the central Sound from the Connecticut shoreline south to the Thalweg is such that the entire water column moves rapidly with the wind component parallel to the coast in the shallow regions, with return flow occupying most of the water column in the deeper portions of the Sound. A similar structure is found in large lakes, such as Lake Erie (Gedney and Lick, 1972). Near-surface currents generated by sea surface slope alone are weak (1 to 2 cm/s or less) and variable, and are still weaker near the bottom.

THE COMPOSITE STRUCTURE OF THE RESIDUAL CIRCULATION

The previous section has isolated the effects on the residual circulation of, in turn, tide, density, wind and sea level slope. In this section we will first consider composite currents for April 1988

and follow this with seasonal variations in the gyral structure in the western and central basins. A final section will consider the structure of the currents derived from observations in the western and central basins.

The composite model system

To systematically develop a picture of the complete gyral circulation, the numerical model was first used to show density currents with tide effects included (Fig. 9), C(A,D). As would be expected from the component pictures of tidal (Fig. 4) C(A) and density (Fig. 7) C(D) effects, the near-surface cyclonic gyres are stronger than in either separate case. Tide and density act together to strengthen the cyclonic gyral circulation. The flow is weaker and more complex at 10 m, again as would be expected from the depth dependence of the component circulations. Near the bottom, there is a small area of noticeably cyclonic flow in the eastern part of the western basin.

When sea level slope and, particularly, wind are added, the picture becomes much more complex. The wind not only tends to generate anticyclonic gyral structures opposite to those of tide and density, but also alters the density structure itself through advection. The result is a non-linear combination of all the effects, which has been numerically decomposed as $C(A,S,W,D) = C(W) + C(S) + C(A) + C(D)$.

With the combined effects of tide, density, wind and sea level slope for April 1988, near the surface, the tide and density generated cyclonic gyre in the central basin is still present (Fig. 10), but it is reduced in size and is confined to the eastern part of the basin. There is an area of irregular anticyclonic flow in the western part of the basin that is separated from the cyclonic gyre by a region of strong north to south flow. The wind appears to predominate in the shallower regions near the Connecticut and Long Island shorelines, where the flow is strongly eastward. The gyre is still present at mid-depth; a strong cyclonic gyre has also developed over Mattituck Sill. Near the bottom there is a tendency toward a large, weak anticyclonic gyre in the central basin, with strong westward flow along the Thalweg through the central and western basins. The wind-driven eastward flow near Connecticut extends to the bottom. There are no clear near-bottom gyral structures in the western basin.

The above shows the major modifications that density and wind stress have on the topographic gyres generated by the tide. Average density stratification strengthens the gyres, while in turn a moderate resultant southeastward wind greatly modifies the structure. Because density, and more particularly wind, are highly variable from month to month, we expect that major changes should occur in other periods.

Seasonal variations

In the previous sections, no offset to long term mean sea level relative to NAVD 1988 was made at Montauk or at The Battery (the eastern and western boundaries of the numerical model). In a series of numerical experiments, an increase in long term mean sea level of 6.7 cm at Montauk relative to The Battery was calibrated to reproduce the net transport in the East River estimated at 310 m³/s by Blumberg and Pritchard (1997). The resulting monthly means of this difference (Montauk minus The Battery) varied from -0.7 to 7.9 cm (Table 1). The mean monthly wind at LaGuardia Airport (LGA) was 2 to 3 m/s east-southeastward during the winter, and weak or north-northeastward in the summer (Table 1).

To investigate differing seasonal density and wind effects, monthly Eulerian residual circulations over the model calibration/validation period from April 1988 to September 1989 were studied. For purposes of comparison, the April 1988 case with tide and density (representative of the yearly average), but with no wind or Montauk-Battery sea level difference (Fig. 9), is considered to represent the baseline gyral structures. These structures consist of a near-surface manifestation in the Western Basin of a circular cyclonic gyre of radius 8 km, while in the Central Basin an ellipse with a easterly directed major axis order 40 km and northerly directed minor axis order 20 km is present.

In comparing the eighteen monthly residual circulations to this base case, three other basic structures emerged. In some months with eastward winds, the Central Basin gyre is shifted to a *reduced* circular feature of radius 10 km situated within the eastern half of the ellipse in the base case. This structure is transformed, when the near-surface Central Basin cyclonic gyre is *pinched*, by mostly along-Sound wind stress, to the east and shrinks to a narrow ellipse, whose major axis is now north-south directed of order 10km and whose minor axis is east-west directed at 4km. In several months, wind effects dominate and both gyres are *absent*.

April 1988 (Fig. 10), with a resultant southeastward wind shrinking the cyclonic gyre in the eastern portion of the Central Basin, represents the reduced structure. For July 1988 under seasonal stratification with a resultant north-northeastward wind of 1.1 m/s and Montauk-Battery sea level difference of 5.1 cm, the near-surface gyres are absent (Fig. 11), replaced by strong eastward flow in the central and westward basins and weaker eastward flow near the Connecticut and Long Island shores. At mid-depth (10m), there is a small anticyclonic gyre in the western part of the central basin. The near-bottom flow is anticyclonic to the north, but weaker than in April, with a general westward component along the Thalweg. For January 1989, without a seasonal thermocline and with a resultant east-southeastward wind of 1.7 m/s and Montauk-Battery sea surface difference of 6.3 cm, this mostly along-Sound wind stress pinches the near-

surface central basin cyclonic gyre to the east (Fig. 12) and shrinks it to a narrow, weak ellipse, whose major axis is now north-south directed of order 10km and whose minor axis is east-west directed of order 4km. A gyre reduced from the base case in size and strength is found at 10m. There is no gyre in the western basin. As in the previous cases, the near-bottom flow near the Thalweg is westward and is anticyclonic to the north, with eastward return flow near Connecticut.

Table 1 summarizes conditions of seasonal stratification, wind speed and direction, and Montauk-Battery sea level difference for the entire 18 month modelling period, together with the mean monthly status of the near-surface central basin gyre.

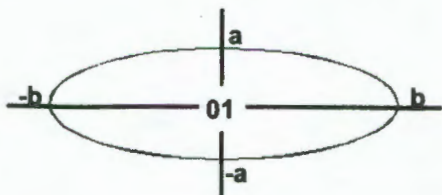
Residual currents derived from observations

Riley (1952) used scattered near-surface current observations to deduce that the upper-layer residual circulation in LIS is characterized by western and central basin gyres, in addition to a general eastward drift. As the above model examination has demonstrated, such a gyral structure is highly variable temporally, and very dependent on the prevailing wind.

Current observations were taken along the boundary between the western and central basin from mid-July to mid-August 1988 at ADCP Station 8 and SUNY Section 3 and from early August and early September in the central basin at ADCP Station 9 and SUNY Section 4, and the mean residual currents for these periods were examined (Fig. 13). The Sound was thermally stratified during the first period, but the thermocline was breaking down during the second. The mean wind for the period was north-northeastward. The model indicates that the central basin gyre was absent in July and August and pinched in September.

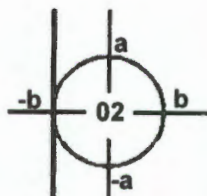
Table 1. Simulated Central Basin Surface Gyral Structure and Associated Thermal Stratification, Windspeed and Direction at LGA, and Montauk-Battery Sea Level Difference

Gyral envelope structure:
Baseline



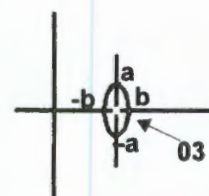
01 = (41.06°N, 72.84°W)
a = 10km B = 20km

Reduced



02 = (41.08°N, 72.66°W)
a = b = 10km

Pinched



03 = (41.06°N, 72.66°W)
a = 5km B = 2km

Stratification:

s= stratified u= unstratified t= transitional ms= mostly stratified mu= mostly unstratified.

Month	Seasonal Thermal Strat.	Resultant Wind Speed (m/s)	Resultant Wind Dir. (deg)	Montauk-The Battery Sea Level Difference (cm)	Gyral Structure
April 1988	t	0.7	323	3.0	reduced
May	ms	0.6	79	1.8	reduced
June	s	1.0	282	3.6	absent
July	s	1.1	200	5.1	absent
August	t	1.5	216	4.8	absent
Sept	mu	1.2	276	4.8	pinched
Oct	u	1.5	270	5.1	pinched
Nov	u	1.8	262	7.2	pinched
Dec	u	2.7	286	7.9	absent
Jan 1989	u	1.7	288	6.3	pinched
Feb	u	1.6	313	5.4	absent
March	u	0.8	16	3.3	pinched
April	t	1.1	301	4.2	reduced
May	ms	0.5	184	-0.7	reduced
June	s	0.4	25	1.2	reduced
July	s	0.2	276	2.7	reduced
Aug	t	0.6	311	3.6	absent
Sept	mu	0.3	79	1.8	reduced

The stations along Stratford Shoal agree qualitatively with the July 1988 near-surface model structure (Fig. 11) and with the tentative picture of the near-bottom circulation. There is a general eastward flow in the upper layers, consistent with the absence of a gyre in July and August. Station 8 in the Thalweg shows residual flow toward the NE at 9 m, which was the nearest surface measurement, with westward flow at 19 m and 34 m, consistent with a dominant gravitational circulation along the Thalweg as also seen in the model structure.

Stations occupied during August to September in the central Sound indicate a possible upper layer anticyclonic gyre with near-surface circulation sweeping around from SUNY stations 4S to 4N not seen in the model. As with the Stratford Shoal Section, the dominant flow in the Thalweg (Station 9) is gravitational circulation, with particularly strong westward flow at depth, which is also present in the model.

DISCUSSION

There is a considerable difference in the deductions one makes about the circulation in the western and central basins of LIS from observations and modelling. The 1990 to 1992 observations alone support the broad general features of LIS circulation discussed by Gordon and Pilbeam (1975), Paskausky and Murphy (1975), and Jay and Bowman (1975). There are indications of possible gyral structures, but other interpretations are also plausible. The observations are too sparse, particularly along-Sound, for any conclusions about spatial scales to be drawn.

By contrast, the model presents a clear picture of the main features of the circulation in the central and western basins under a variety of forcing conditions. The gyral structure emerges as a result of the interaction of a baroclinic tidal flow with topography. Wind stress modifies the near-surface gyral structure considerably, and sometimes eliminates it entirely. It is hypothesized that in the vertically integrated vorticity balance, differential bottom friction by the slope of the bottom perpendicular to the direction of the current is the significant vorticity generation term with vortex stretching acting as a production agency of residual vorticity. In the three-dimensional k component vorticity balance, bottom friction damping and vertical gradients of the horizontal velocity components act to modify the balance over the vertical, such that below 10m no basin scale gyres are present.

There is considerable evidence of seasonality in the 18-month record summarized in Table 1. Weak or irregular net wind stress in the spring of 1988 resulted in a reduced gyre that disappeared in the summer under net SW winds and stratified conditions. In the fall and winter, as seasonal stratification ended and winds shifted to W or NW, the gyre was first pinched, then pinched still further or eliminated, returning to a reduced gyre in the spring of 1989. The situation in the

summer of 1989 was different than that in 1988 in that net winds were much weaker; the reduced gyre persisted through July.

The model depiction in May 1988, the only month with mean westward wind (except for the weaker mean wind in September 1989, when stratification was also much less), was distinctive in that it was the only month in which a near-surface gyre was present in the western basin. The westward wind generated the same qualitative gyral pattern as tide and density, and in fact the central basin gyre was larger and better developed than in any other month. The 10 m fields substantiate changes to the gyral structure with depth in all three major components of the residual circulation whether seasonal stratification is present or not.

In most months, the model near-bottom flow resembled that of the simulated current examples (Figs. 11 and 12), with westward flow through the central basin in the Thalweg, and cyclonic flow to the north, with eastward flow near Connecticut. The major departure from this pattern was in April and May 1989, when modeled bottom flow was much more irregular.

Overall, the model shows the profound alteration that moderate net wind stress makes to the baroclinic circulation pattern in a complex three-dimensional estuary. This is in contrast to the situation in a laterally homogeneous estuary (Hansen and Rattray, 1965), where moderate wind stress alters the magnitude of the gravitational circulation, but does not change its basic character, while a stronger wind against the direction of the upper-layer gravitational circulation alters the direction of flow only very near the surface.

Based on the present hydrodynamic model, minimum gyre scales are estimated to range from 4 to 10 km. These features can only be approximately resolved using the present grid, since at least 10 grid cells necessitating grid spacings from 0.4 to 1 km would be required to fully resolve these features. These spacings are two to five times the resolution of the present numerical grid. Thus, only the general characteristics of the gyres may be inferred from Table 1. Additional numerical experiments with a curvilinear grid of order 0.4 to 1 km grid spacing, are recommended to further elucidate the gyral circulation. A longer modelling period, perhaps several years or more, might further clarify the relationship between wind and gyral structure. On the other hand, detailed observations are needed to substantiate the gyral structure and its variation. Using the present model as a guide, the following ADCP current meter distribution with 10 minute sampling interval is suggested. To study the western basin gyre, two 10 km transects (one north-south and one east-west intersecting at their mid-points at 41°N and 73° 25'W) with station spacing of approximately 5 km would be required. To investigate the central basin gyre one east-west transect extending from (41° 5'N, 72° 40'W) to (41° 5'N, 73° W) and five 10 km north-south

transects intersecting the east west transect at their mid-points at 5 km intervals with station spacing of approximately 5 km would be required.

Additional process studies in which the degree of nonlinearity of momentum equation terms are studied along with alternative density circulation representations appear to be warranted. The development of a vorticity analysis package to complement the Blumberg-Mellor (1980) model should be explored to allow for the identification of the dominant terms in the k component vorticity balance for real estuarine systems under a variety of forcing conditions. In conclusion, continued development of real-time physical oceanographic measurement systems to support operational nowcasting and forecasting of estuarine circulation in conjunction with the above development work holds great promise for the study of residual circulation on a long term basis.

ACKNOWLEDGEMENTS

This work was performed in conjunction with the NOAA Long Island Sound Oceanography Project during the period March 1988 to December 1993 within the Coastal and Estuarine Oceanography Branch, Office of Ocean and Earth Sciences under the supervision of Branch Chiefs Dr. Henry R. Frey (1988 - 1992) and Dr. Bruce B. Parker (1992 - 1993). Dr. Kurt W. Hess, Chief of the Oceanographic Projects Section, provided detailed review of the manuscript and made many valuable suggestions. Dr. Eugene J. Wei greatly assisted with many of the model computations and offered many valuable insights. Mr. Philip H. Richardson was instrumental in salinity and temperature initial and boundary condition development. Ms. Karen L. Earwaker and Mr. Richard W. Bourgerie performed the harmonic and residual water level analyses. Mr. John F. Cassidy developed the horizontal and vertical section graphics. Ms. Brenda W. Via assisted in developing the figures and in preparing the final manuscript.

REFERENCES

Blumberg, A.F. and G.L. Mellor (1980). A Coastal Ocean Numerical Model. In: Mathematical Modeling of Estuarine Physics. Proceedings of an International Symposium, Hamburg, August 24 - 26, 1978. J. Sündermann and K.P. Holz, Eds., Springer-Verlag, Berlin.

Blumberg, A.F. and G.L. Mellor (1987). A Description of a Three-Dimensional Coastal Ocean Circulation Model., In: Three-Dimensional Coastal Ocean Models, Coastal and Estuarine Sciences, 4, N. Heaps, Ed.; American Geophysical Union, Washington, D.C., 1-16.

Blumberg, A.F. and H.J. Herring (1987). Circulation Modeling Using Orthogonal Curvilinear Coordinates, In: Three-Dimensional Models of Marine and Estuarine Dynamics, J.C.J. Nihoul and B.M. Jamart, Eds., Elsevier Publishing Company, 55-88.

Blumberg, A.F. and D.W. Pritchard (1997). Estimates of the Transport through the East River, New York, Journal of Geophysical Research, 102:5685-5703.

Galperin, B., L.H. Kantha, S. Hassid, and A. Rosati (1988). A Quasi-Equilibrium Turbulent Energy Model for Geophysical Flows, Journal of the Atmospheric Sciences, 45 (1) : 55-62.

Garvine, R.W. (1986). The Role of Brackish Plumes in Open Shelf Waters. In: The role of Freshwater Outflow in Coastal Marine Ecosystems, NATO ASI Series, Vol. G7, pp. 47-65.

Gedney, R.T. and W. Lick (1972). Wind-driven Currents in Lake Erie. Journal of Geophysical Research 70:2714-23.

Godin, G. (1972). The Analysis of Tides. Liverpool University Press-University of Toronto Press, 264pp.

Gordon, R.B. and C.C. Pilbeam (1975). Circulation in Central Long Island Sound. Journal of Geophysical Research 80:414-22.

Hansen, D.V. and M. Rattray Jr. (1965). Gravitational Circulation in Straits and Estuaries. Journal of Marine Research 23:104-22.

Hsu, S.A. (1986). Correction of Land-based Wind Data for Offshore Applications: a further evaluation. Journal of Physical Oceanography 16: 390-394.

Ianniello, J.P. (1981). Tidally Induced Residual Circulation in Long Island Sound. Estuarine Coastal and Marine Science 12:177-91.

Jay, D.A. and M.J. Bowman (1975). The Physical Oceanography and Water Quality of New York Harbor and Western Long Island Sound. MSRC, SUNY Stony Brook, TR #23, 71 pp.

Large, W.G. and S. Pond (1981). Open Ocean Momentum Flux Measurements in Moderate to Strong Winds. Journal of Physical Oceanography 11:324-326.

- Li, C. And J. O'Donnell (1997). Tidally Driven Residual Circulation in Shallow Estuaries with Lateral Depth Variation. Journal of Geophysical Research 102:27915-27929.
- Mellor, G.L. and T. Yamada (1982). Development of a Turbulence Closure Model For Geophysical Fluid Problems, Rev. Geophys. Space Phys., 20, 851-875.
- Murphy, D.L. (1980). A Numerical Investigation into the Physical Parameters which Determine Residual Drift in Long Island Sound, PhD Dissertation, University of Connecticut, 181pp.
- NOS (1990). Long Island Sound Oceanography Project: 1988-1990. NOS Oceanographic Circulation Survey Report No. 10, 40 pp.
- Paskausky, D.F. (1977). Net Drift in an Atypical Estuary, Long Island Sound. Environmental Management 4:331-342.
- Paskausky, D.F. and D.L. Murphy (1976). Seasonal Variation of Residual Drift in Long Island Sound. Estuarine, Coastal and Shelf Science 4:513-22.
- Pritchard, D.W. (1990). A Brief Description of the Circulation in Long Island Sound, Letter Report to USEPA, Washington, DC.
- Ridderinkhof, H. and J.T.T. Zimmerman (1990). "Residual Currents in the Western Dutch Wadden Sea", in Residual Currents and Long-term Transport, R.T. Cheng (ed), Springer Verlag, New York.
- Riley, G.A. (1952). Hydrography of Long Island and Block Island Sounds. Bulletin of Bingham Oceanographic Collection 13:5-39.
- Riley, G.A. (1956). Oceanography of Long Island Sound, 1952-1954. Bulletin of Bingham Oceanographic Collection 15:15-46.
- Robinson, I.S. (1981). Tidal Vorticity and Residual Circulation, Deep-Sea Research 3:195-212.
- Schmalz, R.A. (1990). "A Review of Estuarine, Shelf and Ocean Hydrodynamics", In: Proceedings of Estuarine and Coastal Modeling Conference, Nov. 15-17, 1989, Newport, Rhode Island, ASCE, New York, New York.

Schmalz, R.A. (1992). "Simulation of Three-Dimensional Hydrodynamics in Long Island Sound: Annual Time scales", In: Proceedings of 2nd International Conference on Estuarine and Coastal Modeling, Nov. 13-15, 1991, Tampa, Florida, ASCE, New York, New York.

Schmalz, R.A. (1994). Long Island Sound Oceanography Project, Summary Report Volume 1: Application and Documentation of the Long Island Sound Three-Dimensional Circulation Model. NOAA Technical Report NOS OES 003, Silver Spring, Maryland. 77 pp.

Schmalz, R.A., M.F. Devine and P.H. Richardson (1994). Long Island Sound Oceanography Project, Summary Report Volume 2: Residual Circulation and Thermohaline Structure. NOAA Technical Report NOS OES 003, Silver Spring, Maryland. 191 pp.

Sun, L. C. (1992). "A Numerical Model Simulation of Tidal Currents in Long Island and Block Island Sounds", In: Proceedings of 2nd International Conference on Estuarine and Coastal Modeling, Nov. 13-15, 1991, Tampa, Florida, ASCE, New York, New York.

Valle-Levinson, A. and R.E. Wilson (1994a). Effects of Sill Bathymetry, Oscillating Barotropic Forcing and Vertical Mixing on Estuary/Ocean Exchange, Journal of Geophysical Research, 99:5149-5169.

Valle-Levinson, A. and R.E. Wilson (1994b). Effects of Sill Processes and Tidal Forcing on Exchange in Eastern Long Island Sound, Journal of Geophysical Research, 99:12667-12681.

Wei, Eugene J. (1993). "Development of a Long Island Sound Tidal Circulation and Water Level Atlas", In: Advances in Hydroscience and Engineering: Proceedings of the 1993 International Conference on Hydroscience and Engineering, June 7-11, 1993, Washington, DC, University of Mississippi, Oxford, Mississippi.

Wilson, R.E. (1976). Gravitational Circulation in Long Island Sound. Estuarine Coastal and Marine Science 4:443-53.

Zimmerman, J.T.F. (1980). Vorticity Transfer by Tidal Currents Over an Irregular Topography, Journal of Marine Research 38:601-630.

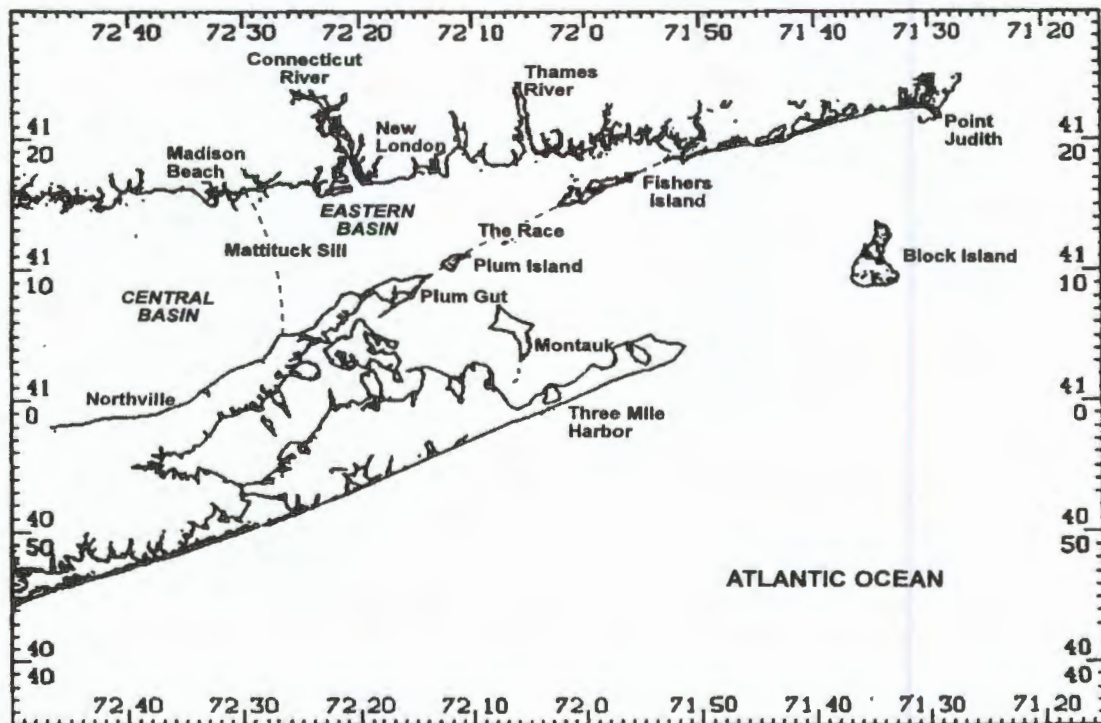
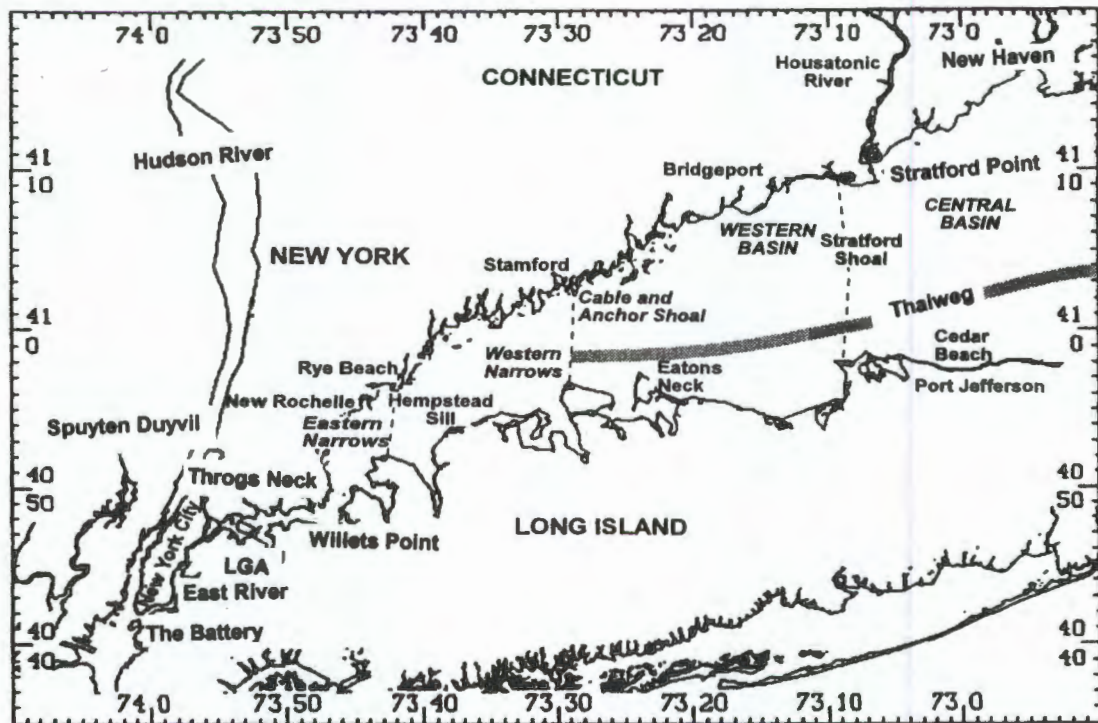


Figure 1. Long Island Sound Basin Classification

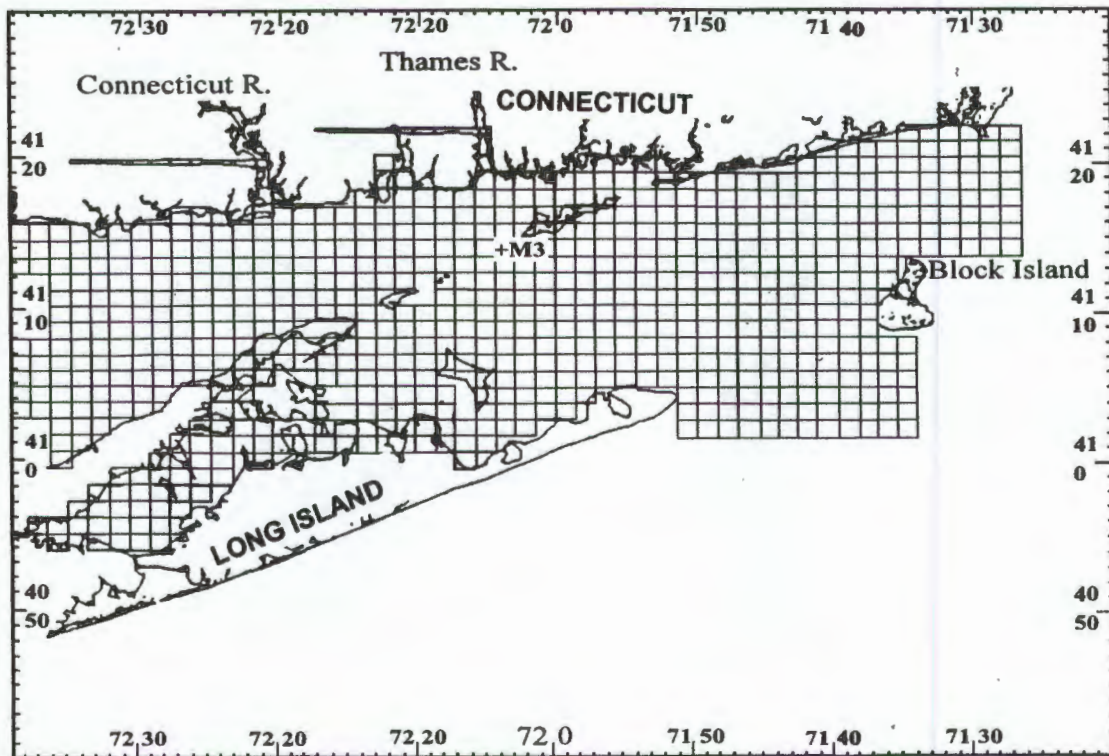
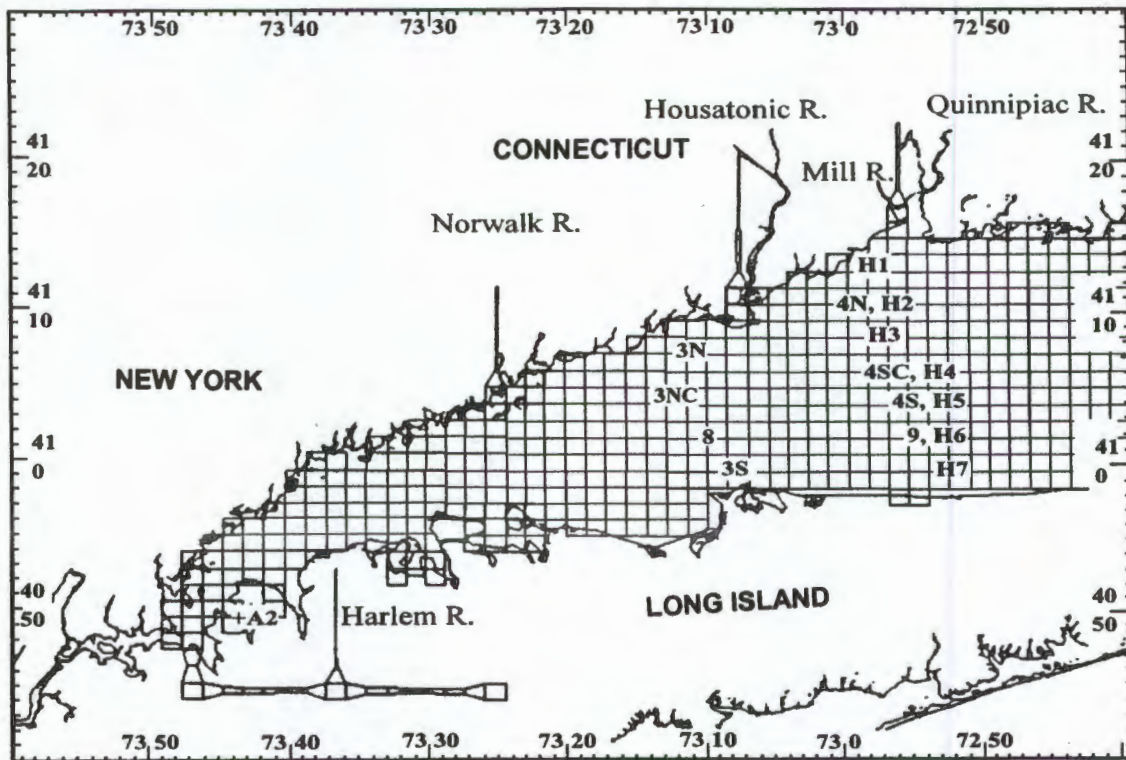


Figure 2. Long Island Sound Hydrodynamic Model Grid

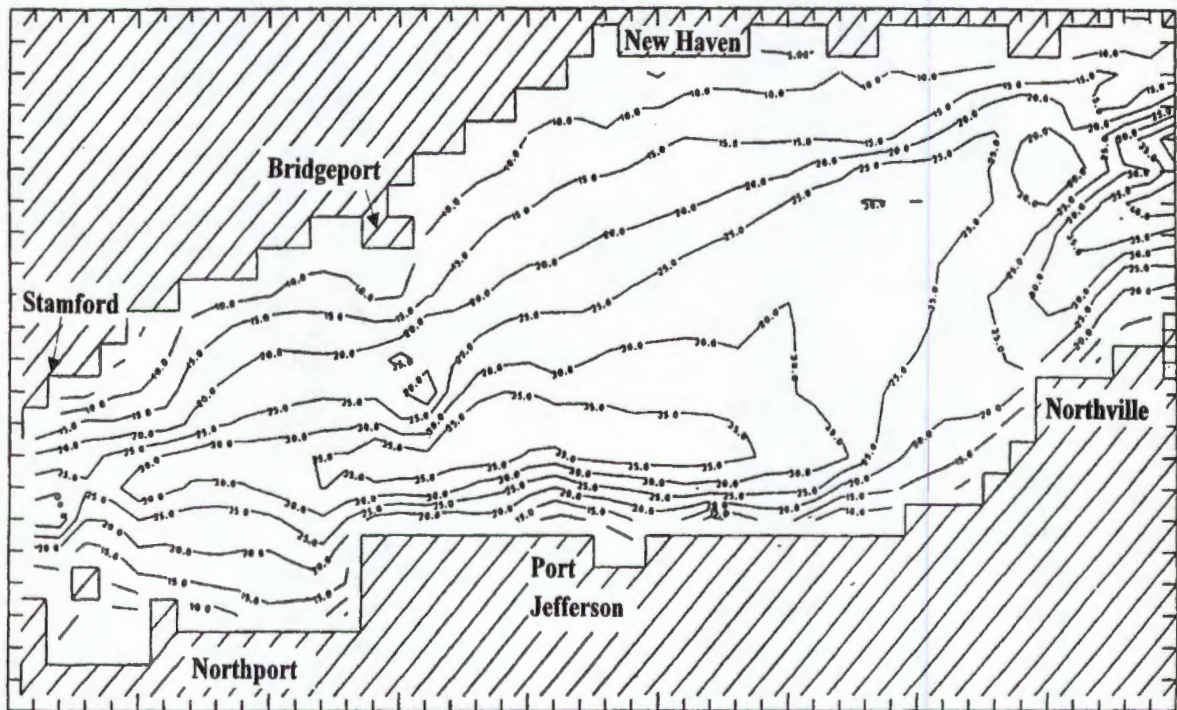


Figure 3. Long Island Sound Hydrodynamic Model Bathymetry: Western and Central Basins (Contour Interval 5m)

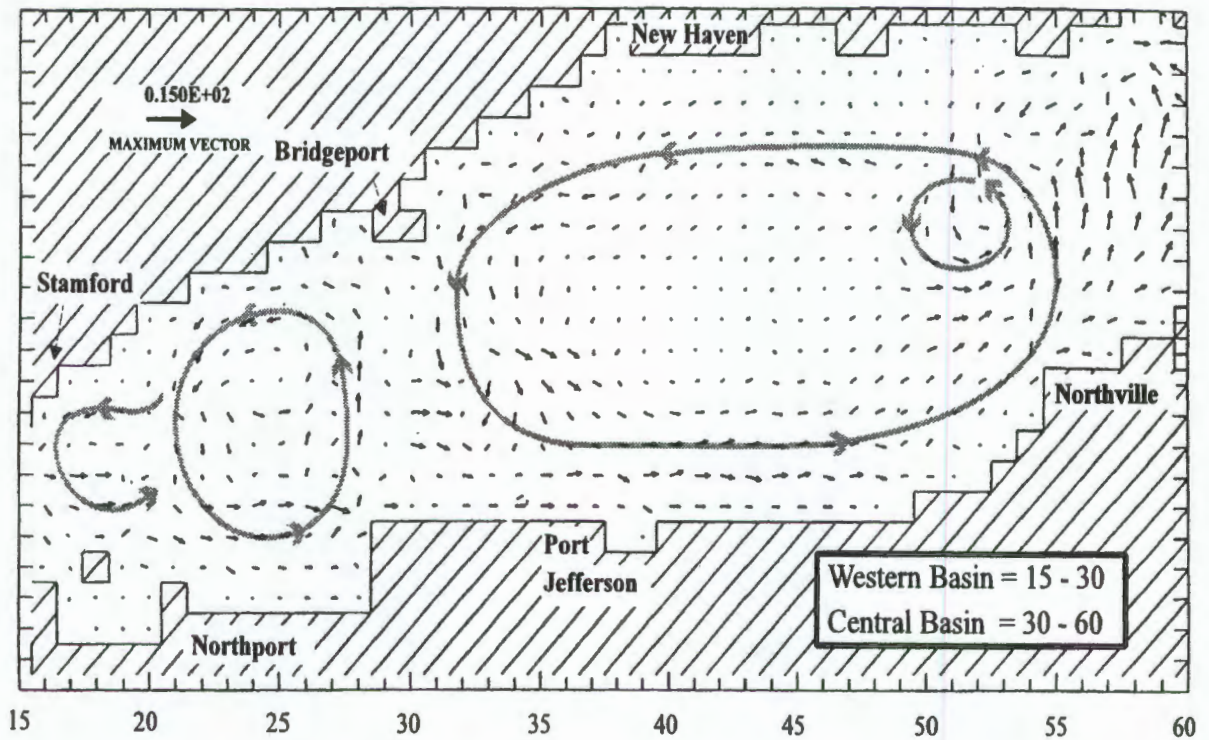


Figure 4a. Simulated Astronomical Tide Eulerian Residual Currents (cm/s)
(2m below surface) April 1988

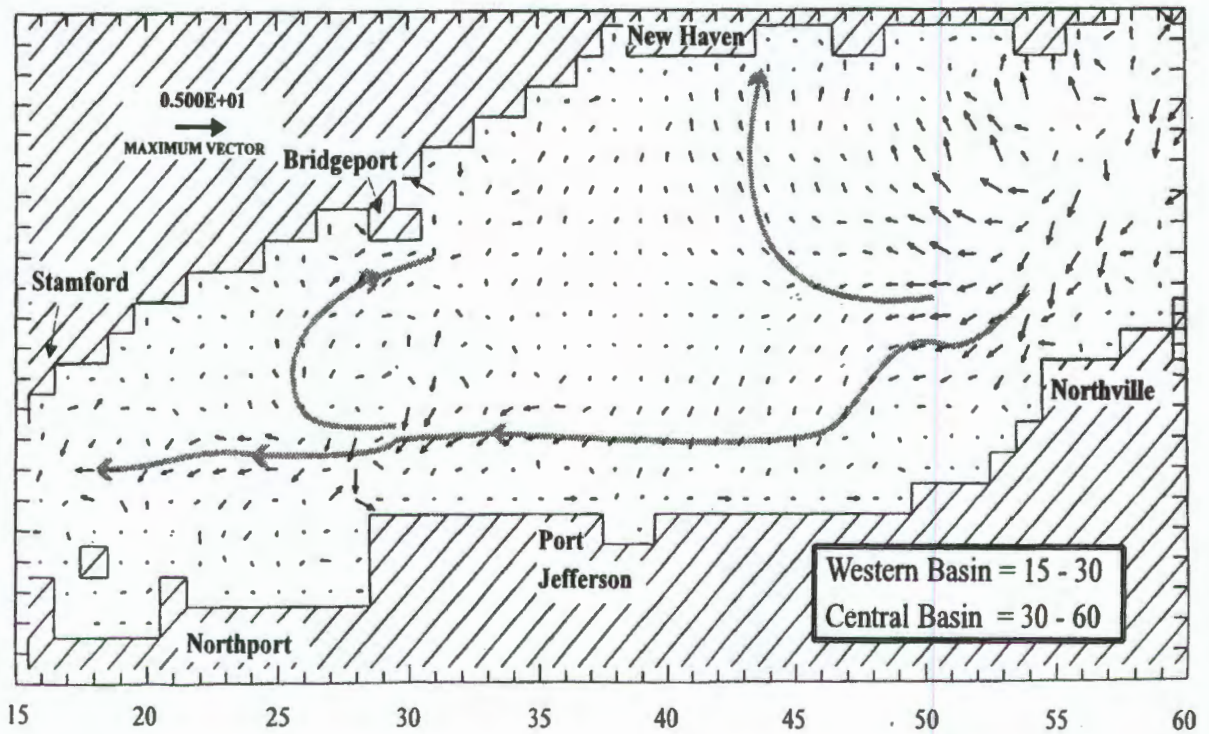
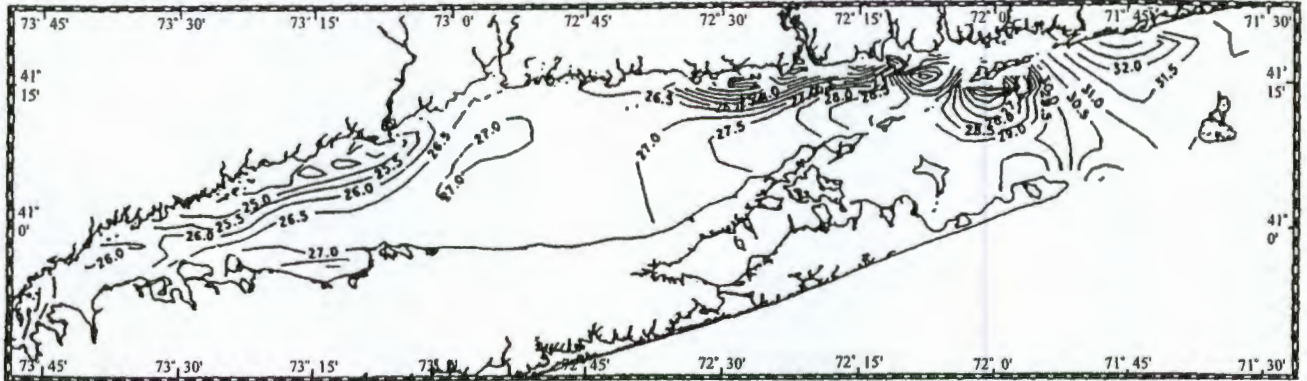


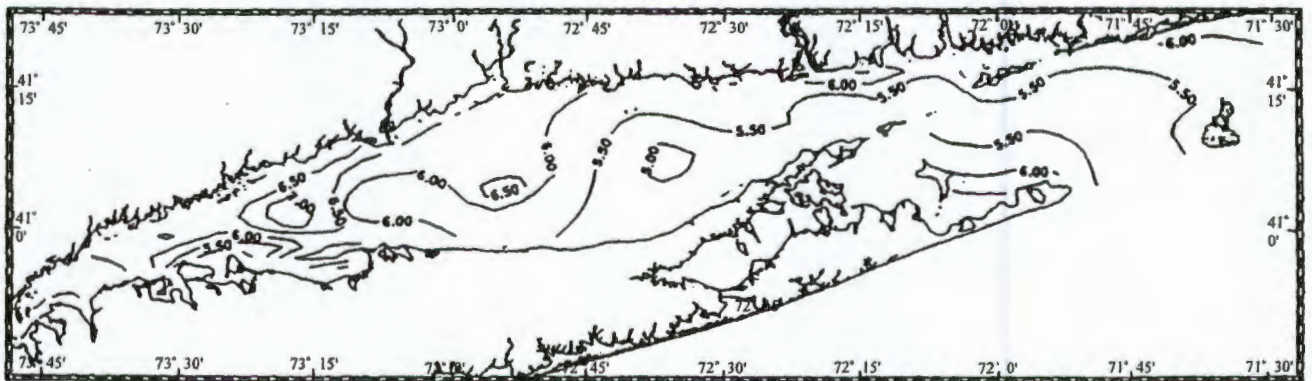
Figure 4b. Simulated Astronomical Tide Eulerian Residual Currents (cm/s)
(2m above the bottom) April 1988

Note broad streamlines are hand-drawn to indicate the general circulation pattern.

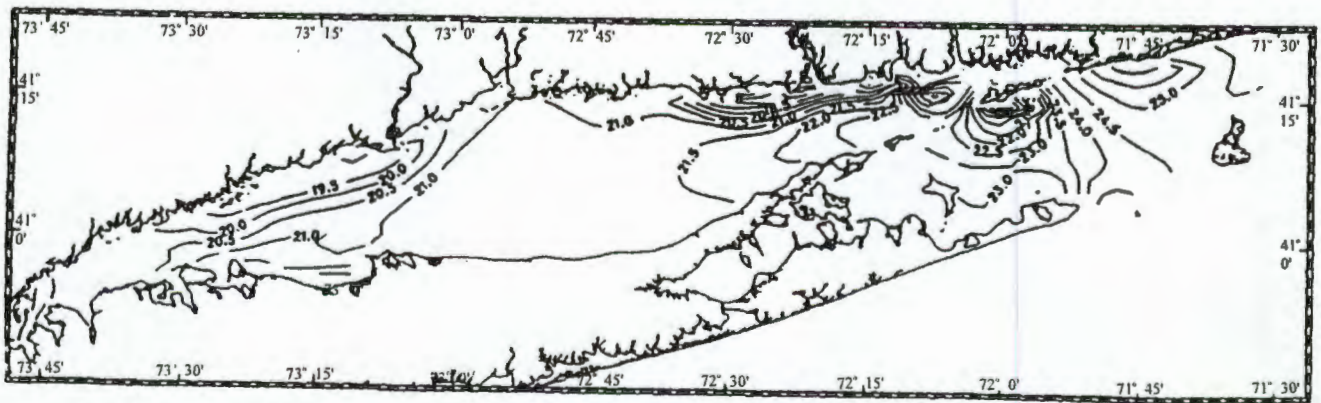
Surface Salinity [Psu]



Surface Temperature [C]



Surface Density [σ_t]



April 4 - 7, 1988

Figure 5. Near-Surface Observational Salinity, Temperature, and Sigma-t Maps: April 1988

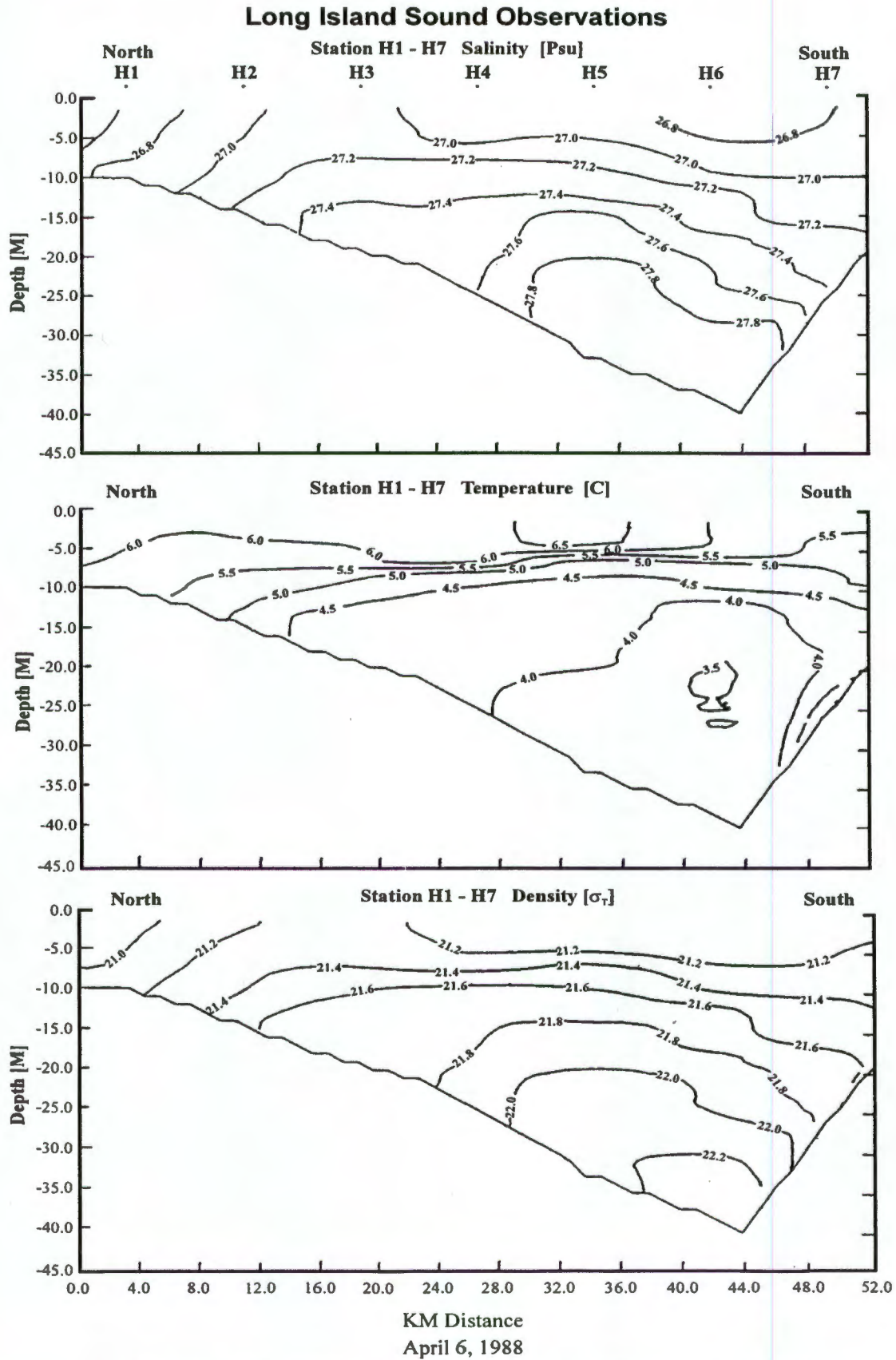


Figure 6. H1 - H7 North-South Observational Section: April 1988

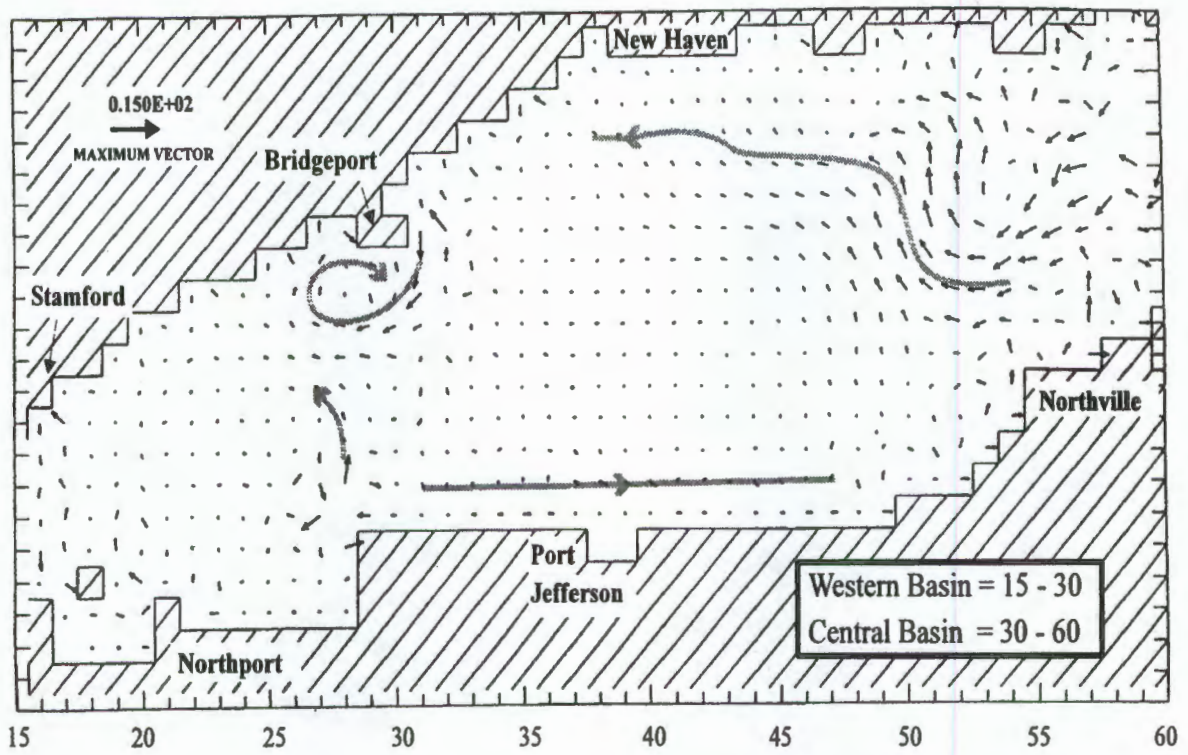


Figure 7a. Simulated Density Eulerian Residual Currents (cm/s)
(2m below surface) April 1988

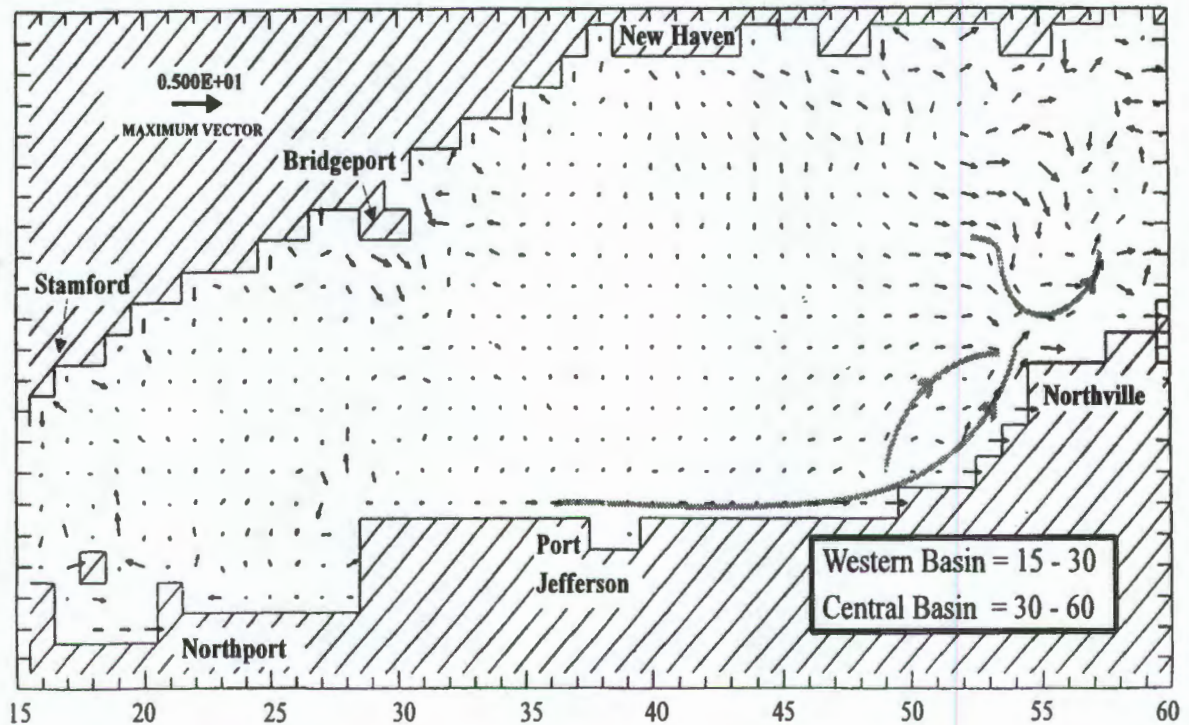


Figure 7b. Simulated Density Eulerian Residual Currents (cm/s)
(2m above the bottom) April 1988

Note broad streamlines are hand-drawn to indicate the general circulation pattern.

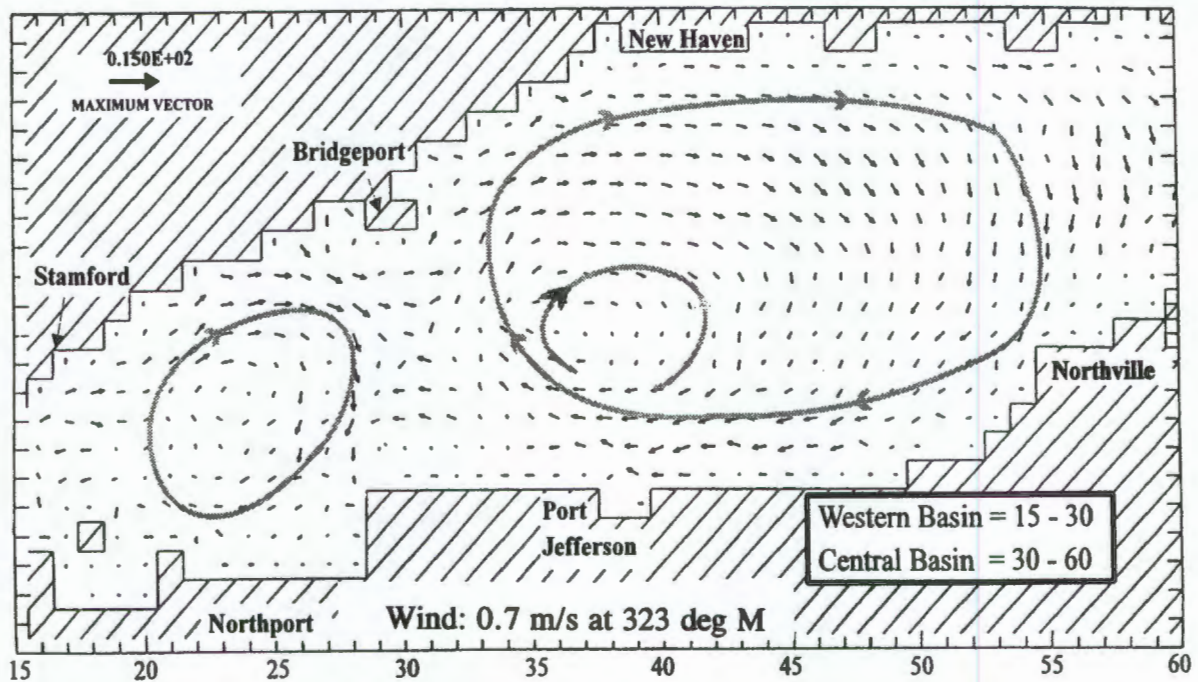


Figure 8a. Simulated Local Wind Eulerian Residual Currents (cm/s)
(2m below surface) April 1988

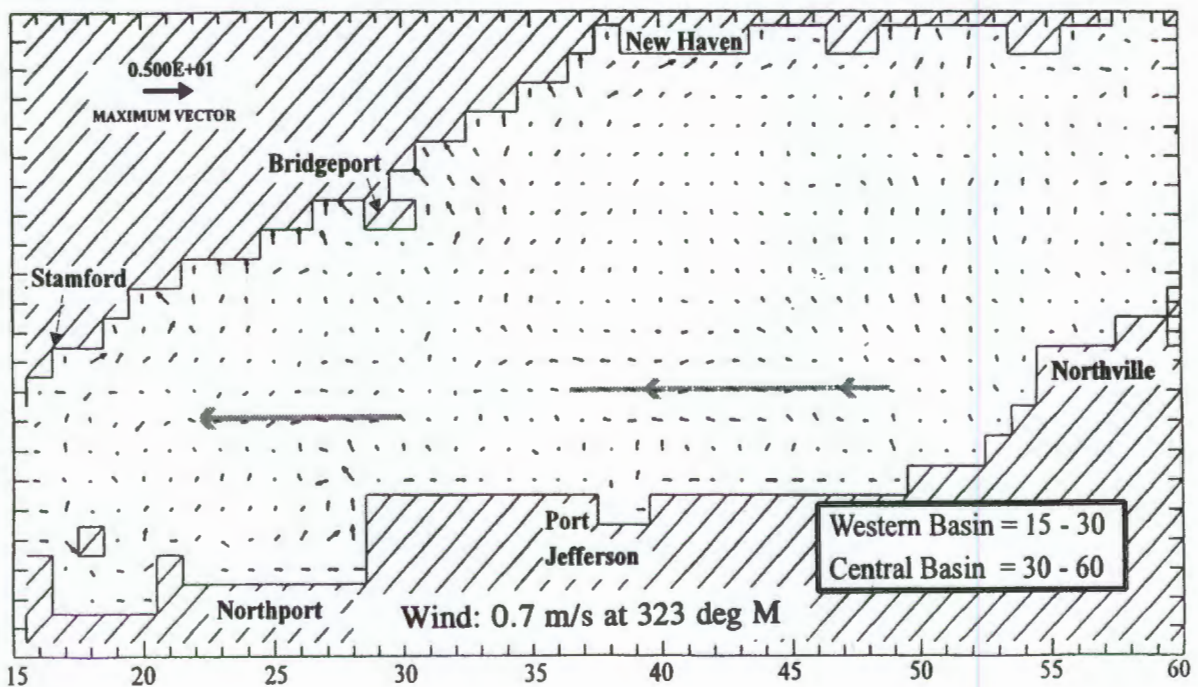


Figure 8b. Simulated Local Wind Eulerian Residual Currents (cm/s)
(2m above the bottom) April 1988

Note broad streamlines are hand-drawn to indicate the general circulation pattern.

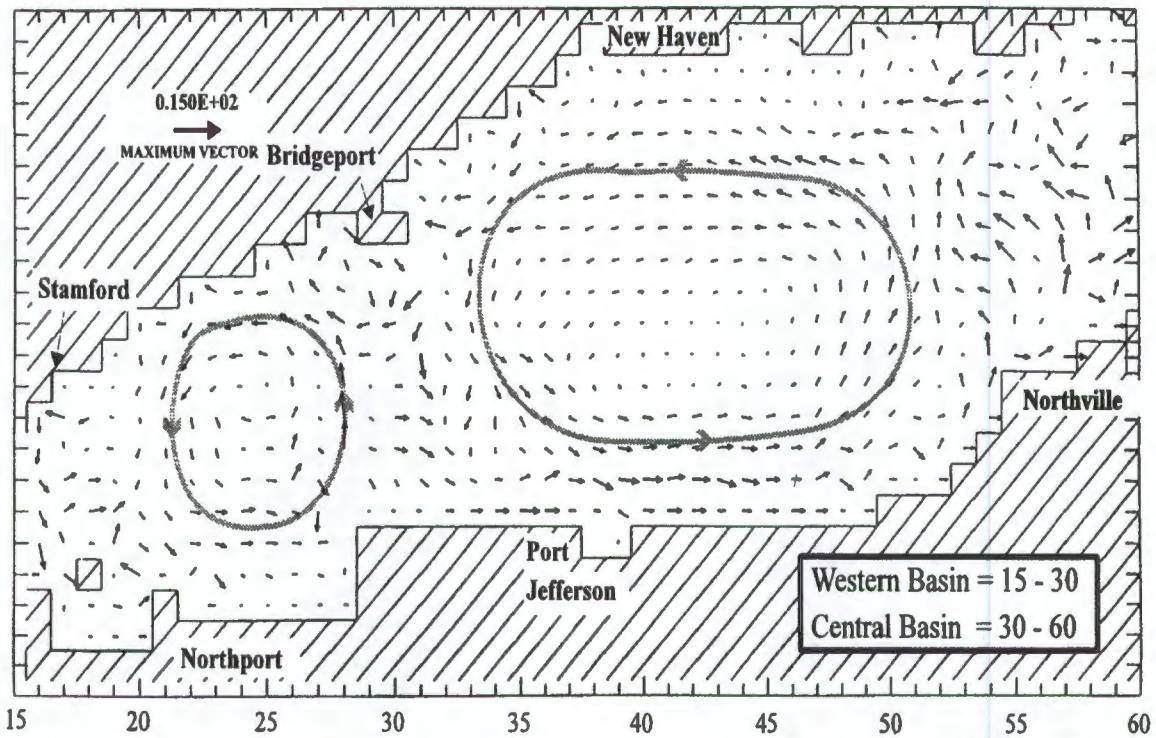


Figure 9a. Simulated Astronomical Tide Plus Density Eulerian Residual Currents (cm/s)
(2m below surface) April 1988

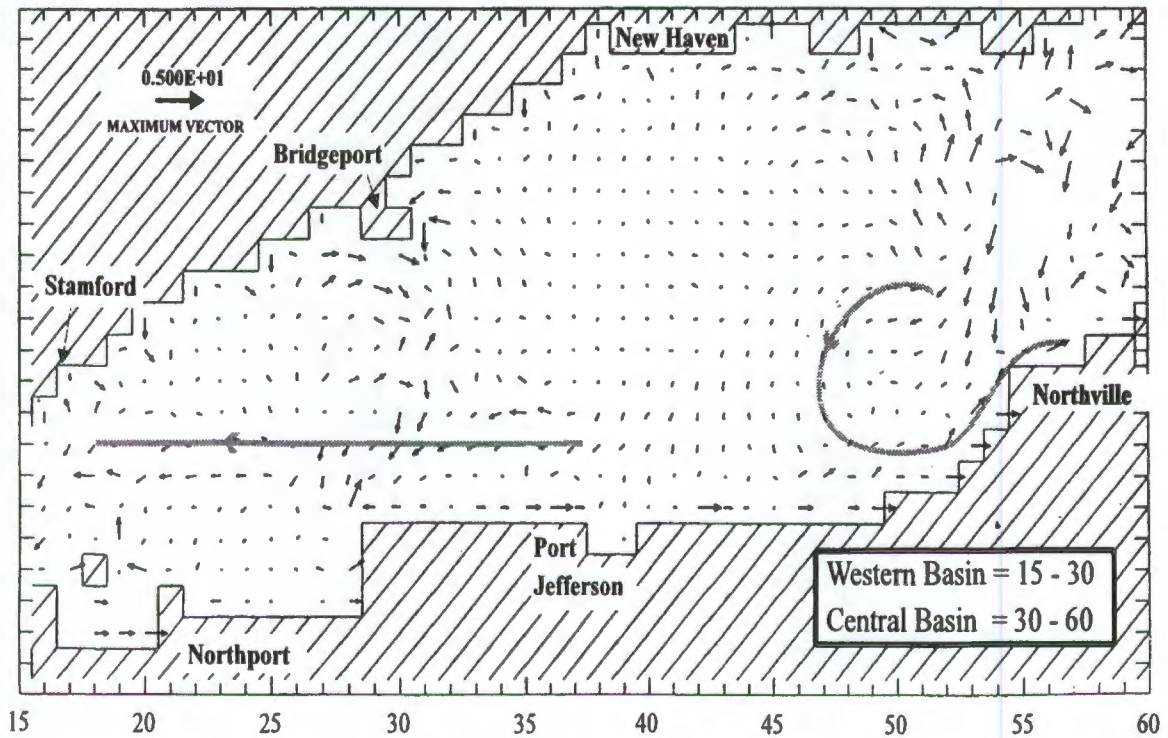


Figure 9b. Simulated Astronomical Tide Plus Density Eulerian Residual Currents (cm/s)
(2m above the bottom) April 1988

Note broad streamlines are hand-drawn to indicate the general circulation pattern.

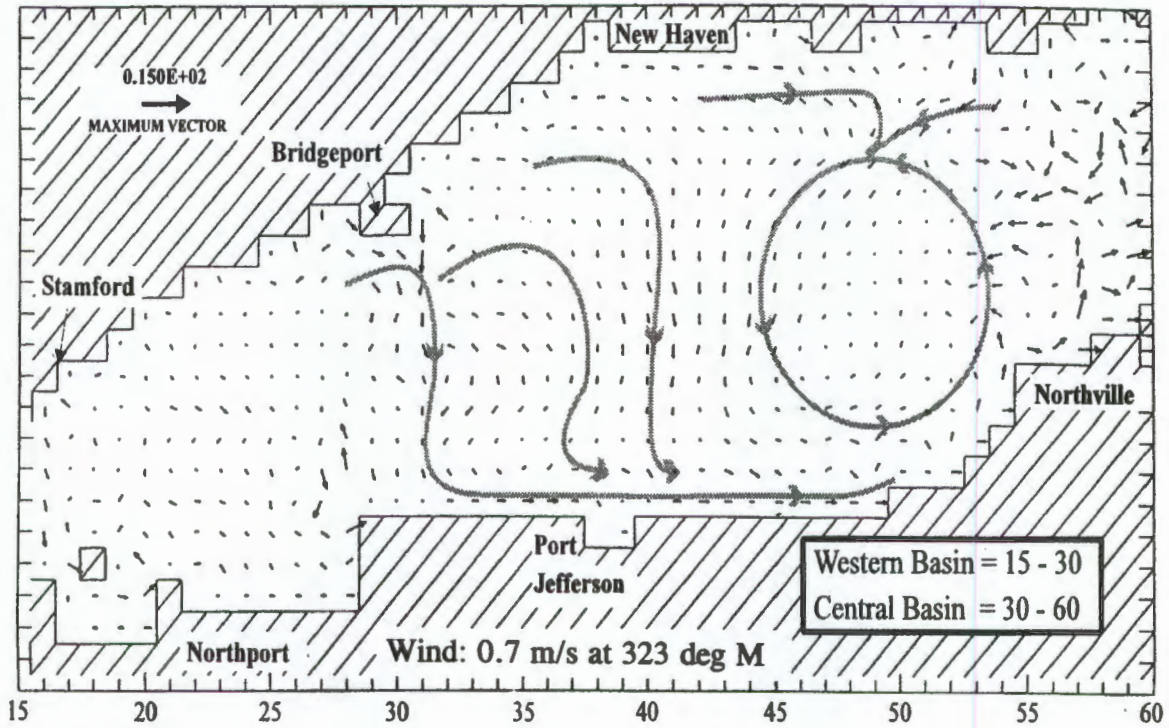


Figure 10a. Simulated Eulerian Residual Currents (cm/s) (2m below surface) April 1988

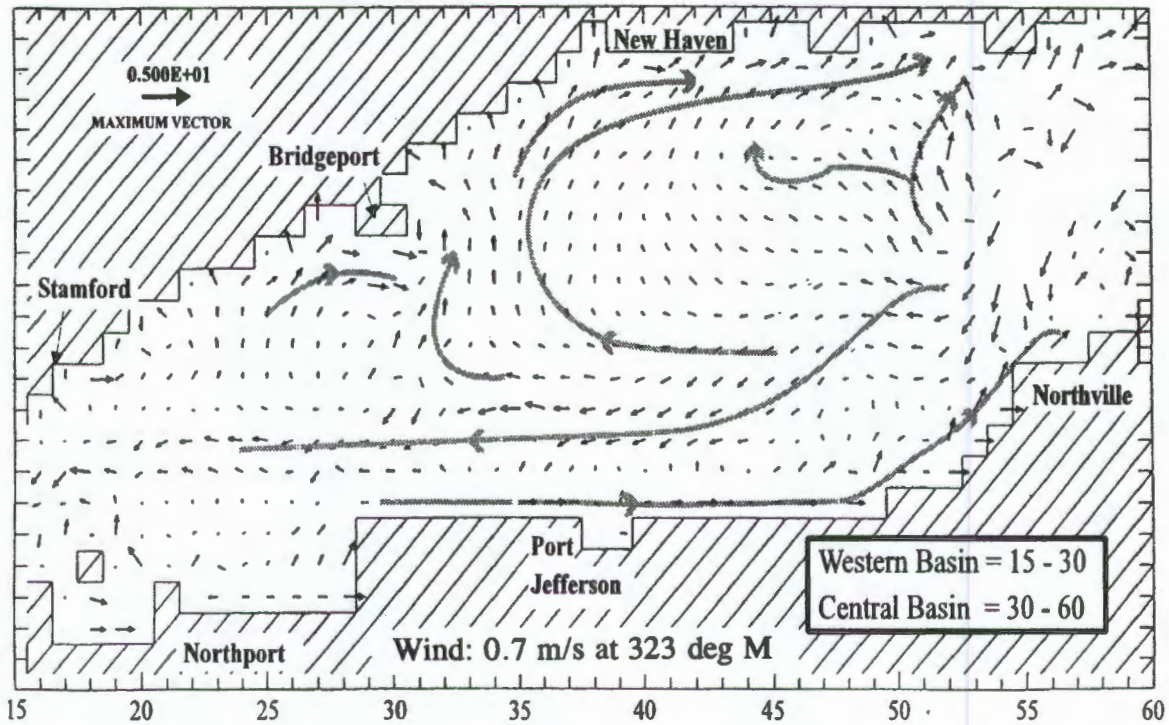


Figure 10b. Simulated Eulerian Residual Currents (cm/s) (2m above the bottom) April 1988

Note broad streamlines are hand-drawn to indicate the general circulation pattern.

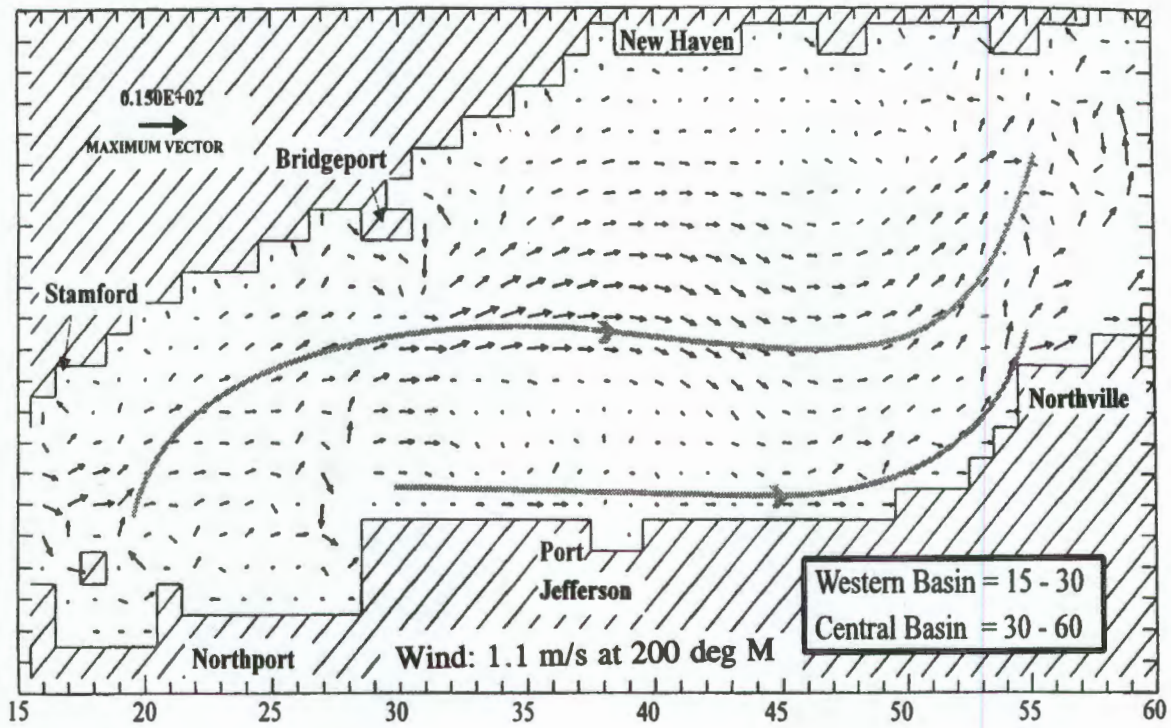


Figure 11a. Simulated Eulerian Residual Currents (cm/s) (2m below surface)
July 1988

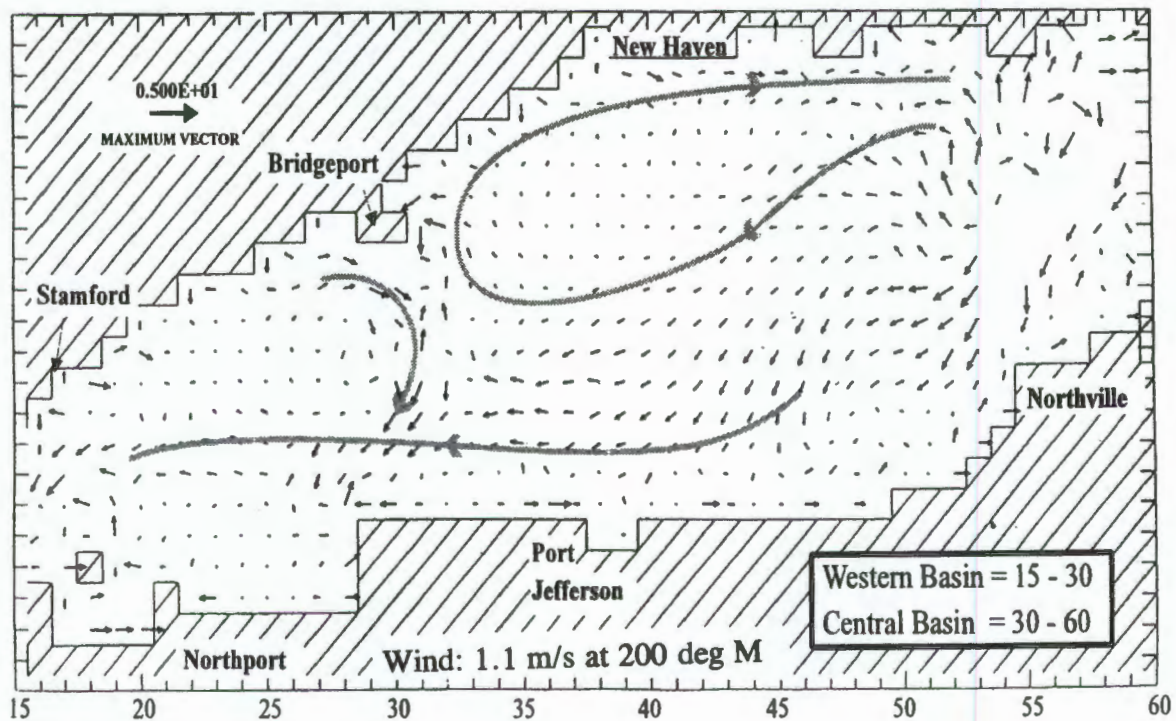


Figure 11b. Simulated Eulerian Residual Currents (cm/s) (2m above the bottom)
July 1988

Note broad streamlines are hand-drawn to indicate the general circulation pattern.

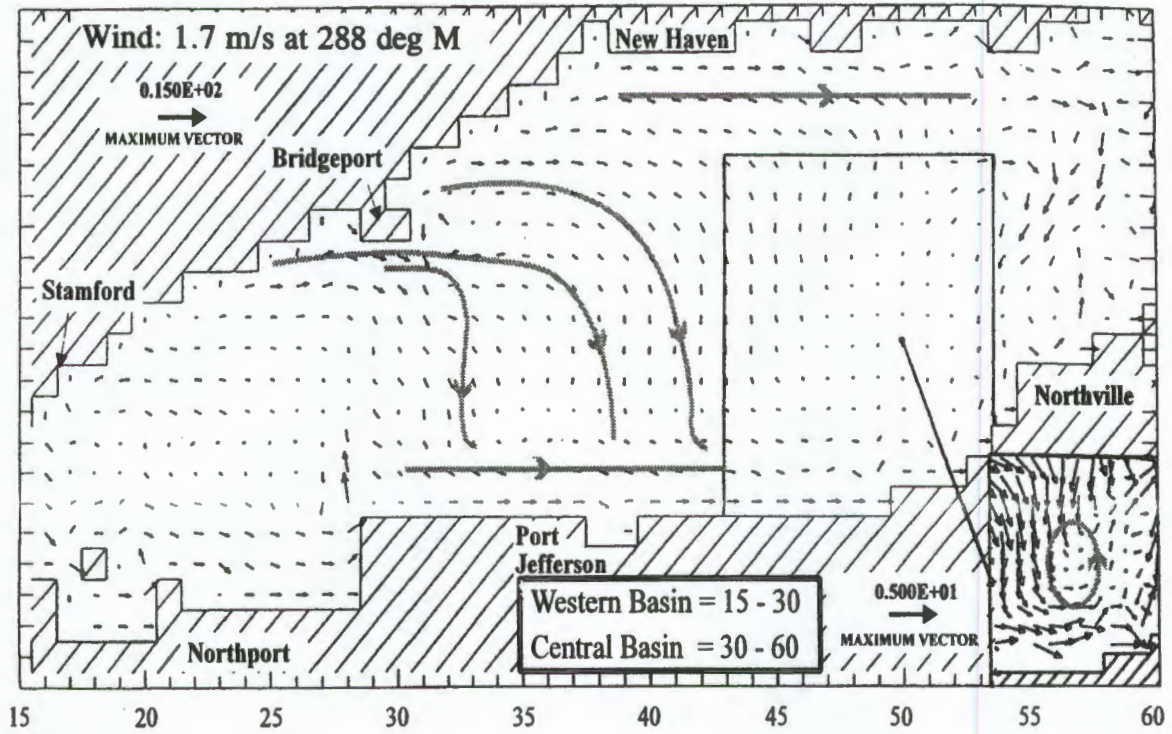


Figure 12a. Simulated Eulerian Residual Currents (cm/s) (2m below surface) January 1989

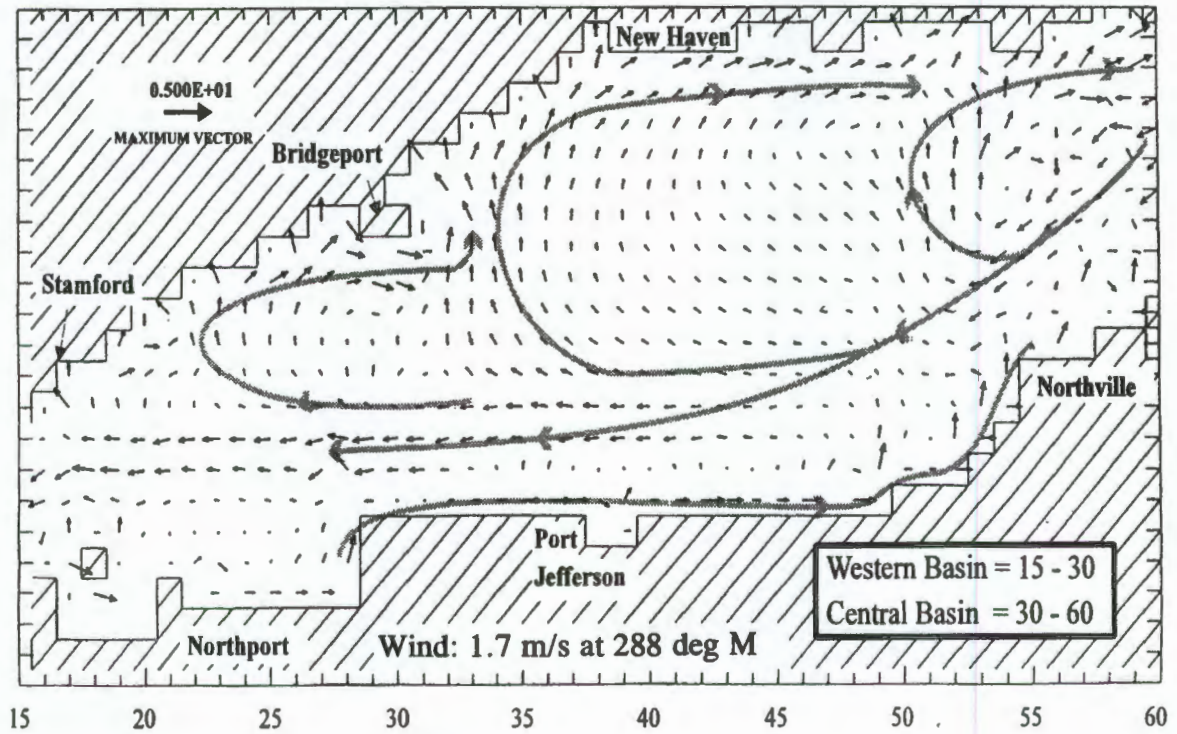
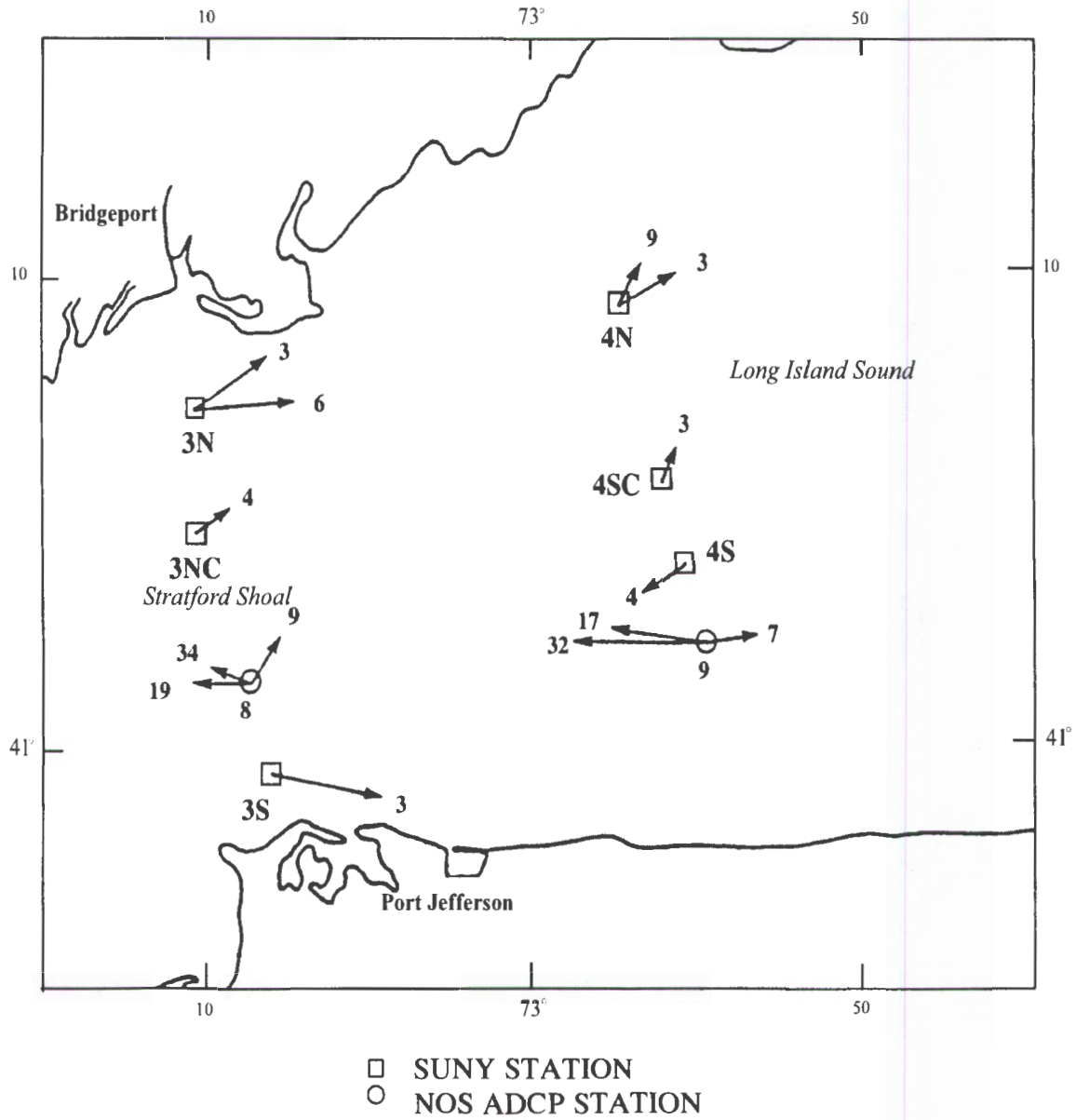


Figure 12b. Simulated Eulerian Residual Currents (cm/s) (2m above the bottom) January 1989

Note broad streamlines are hand-drawn to indicate the general circulation pattern.



The length of the arrows represents a one day translation. The depth of the current in meters is indicated at the head of the arrow. Current strength at 32m at NOS ADCP Station 9 corresponds to 5 cm/s.

Figure 13. Central Basin Residual Currents at NOS ADCP and SUNY Stations

CONCLUDING REMARKS

The NOS Long Island Sound Oceanography Project provided EPA with three-dimensional residual circulation fields (hourly averaged) over an eighteen month period for use in water quality modeling. A monitoring program was also established by EPA to monitor the impact on dissolved oxygen of management decisions. A Long Island Sound Office was established in cooperation with the New York Sea Grant Office to promote interest and further involve the public in the improvement of the Long Island Sound resource (www.epa.gov/region01/eo/lis). On March 5, 2001 the Long Island Sound Office released a new Long Island Study Report entitled: *Sound Health 2001: Status and Trends in the Health of Long Island Sound*. The report concludes that while great progress has been made in pollutant load reduction and habitat restoration, much remains to be accomplished.

